Chapter 3

DRYING SHRINKAGE AND CREEP IN CONCRETE: A SUMMARY

This chapter presents a review on the delayed strains in concrete. More specifically, we will focus our attention on the time-dependent deformations due to drying and creep phenomena in cementitious materials. Their origins and consequences, as well as the main factors involved and their mathematical treatment will be addressed. Drying shrinkage may be defined as the volume reduction that concrete suffers as a consequence of the moisture migration when exposed to a lower relative humidity environment than the initial one in its own pore system. For workability purposes the amount of water added to the mixture is much higher than that strictly needed for hydration of concrete (Neville, 2002; Mehta & Monteiro, 2006). It is well-known that almost half of the water added to the mixture will not take part of the hydration products and as a consequence it will not be chemically bound to the solid phase. Accordingly, when the curing period is completed and concrete is subjected to a low relative humidity (RH) environment, the resulting gradient acts as a driving force for moisture migration out of the material, followed by a volume reduction of the porous material. In a similar way, swelling (i.e. volume increase) occurs when there is an increase in moisture content due to absorption of water (Acker, 2004). On the other hand, creep is the time-dependent strain that occurs due to the imposition of a constant stress in time. Its dual mechanism is called relaxation, which is the time-dependent reduction of the stress due to a constantly maintained deformation level in time. Creep and shrinkage of concrete are described in the same chapter because these phenomena have some important common features: they both have its origin within the hardened cement paste (HCP), the resulting strains are partially reversible, the evolution of deformations is similar (figure 3.1) and finally the factors affecting them usually do so in a similar way in both cases (Mehta & Monteiro, 2006).

Drying shrinkage and creep of concrete have been given a great deal of attention during the past century, especially during the 70's and 80's, driven by the need to quantify the long-term deformation and behavior of nuclear reactor containments (Bazant, 1984; Bazant, 1988; Granger, 1996; Shah & Hookham, 1998; Ulm *et al.*, 1999b; Acker & Ulm, 2001; Witasse, 2000). A large amount of experimental data has been collected over the years and their mechanisms are relatively well understood. Nonetheless, some discrepancies or coexisting theories still exist for explaining some specific features of creep and shrinkage, as will be underlined in the next paragraphs. The work in this thesis will revisit and put a different light into some of these aspects, in this case from a meso-scale point of view. It should be noted that not only the shrinkage strains are important regarding drying of concrete. Another vital issue in durability

mechanics is the ability to predict the internal moisture conditions within the material, since most degradation processes are highly dependent on the moisture content, as for example the ingress of detrimental ions or the vulnerability of a structure to freeze-thaw cycles in cold weather conditions.

The chapter is organized as follows. First, a description of the main drying and shrinkage mechanisms will be presented, together with the main factors affecting shrinkage strains and some other important experimental evidence, with emphasis on the effect of aggregates and drying-induced microcracking. Afterwards, a short summary on the most important experimental features of creep in concrete will be addressed. Section 3.3 will be devoted to discuss some code-type formulas proposed to evaluate drying shrinkage and creep strains. Finally, a complete survey of numerical models for drying shrinkage and its mathematical treatment will be presented, together with the most salient mathematical characteristics of creep modeling.

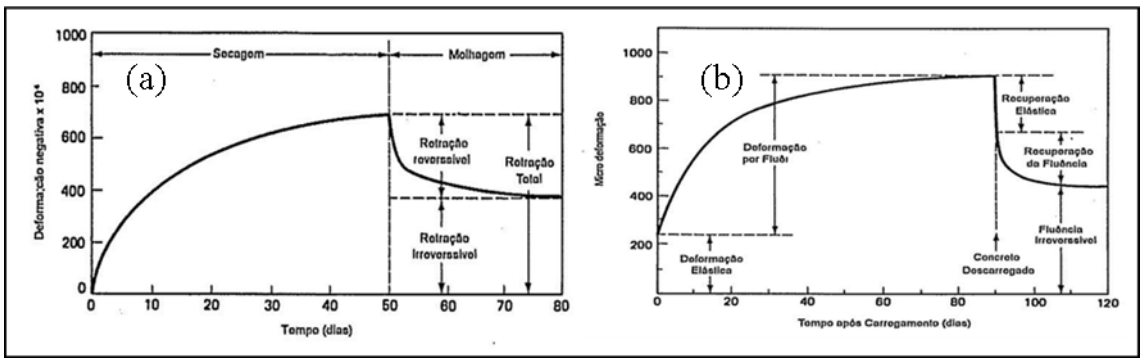

Figure 3.1. Longitudinal strains as a function of time for (a) a drying shrinkage experiment (drying and wetting cycle) and (b) a creep test showing increasing strain at loading and partial recovery upon unloading (from Mehta & Monteiro, 2006).

Delayed strains in concrete may be of various origins, some of them out of the scope of this thesis. Nonetheless it is worthy to briefly describe them in order to clearly delimit this review and also the applicability of the model presented in the next chapters. Regarding shrinkage strains, volume reductions during hydration, such as thermal shrinkage, plastic shrinkage and autogeneous shrinkage are the main early volume changes referred to in the literature (see e.g. Kovler & Zhutovsky, 2006). As they all occur during the hydration period, the time scale is much smaller than that of basic or drying creep and drying shrinkage and they need a different treatment, since the degree of hydration is a key factor in these cases. Thermal shrinkage is the volume reduction due to the decrease in temperature after hydration heat is dissipated (see e.g. Granger, 1996). Autogeneous or self-desiccation shrinkage occurs in moisture-sealed conditions as water is internally removed from the capillary pores by chemical combination during hydration (Hua *et al.*, 1997; Norling, 1997; Acker, 2004), and is mostly important in high performance concretes, due to the low w/c ratio used in the mixes (Acker, 2001). Swelling of concrete may occur when cured under water, due to absorption from the cement paste (Neville, 2002; Kovler, 1999), although it is in general not of practical importance. Plastic shrinkage occurs when water is lost, due to either evaporation on the surface or suction by a drier lower layer, while concrete is in the plastic state, i.e. the setting time has not been completed (Bazant, 1988). It is thus emphasized that deformations occurring during the hydration period (often referred to early age changes) will not be further considered in this thesis. Another type of shrinkage strain, this one occurring at the same time scale as drying shrinkage is the

carbonation shrinkage, that is mainly due to the diffusion of carbon dioxide (CO_2) into the capillary pores, reacting with portlandite (CH) to form carbonates ($CaCO_3$) (Bazant, 1988; Ferreti & Bazant, 2006). Accordingly, there are other creep strains, such as transitional thermal creep, which is the strain that occurs when there is a temperature raise in concrete while under load, or wetting creep, due to an increase in moisture content (Bazant, 1988), which will left out of this review.

3.1. Experimental evidence: drying, cracking and shrinkage

3.1.1 A brief review of drying and shrinkage mechanisms in concrete

The mechanisms involved in the drying process are complex and are often interrelated. This is mainly due to the wide range of the pore size distribution in standard concrete mixes, which determines, to a large extent, the different transport mechanisms during drying. In turn, the pore system evolves in time as a result of hydration and aging. Figure 3.2 shows the typical pore size range present in standard concrete. Moisture transport within the porous solid involves liquid water as well as water vapor (Bear & Bachmat, 1991), and mechanisms such as permeation due to a pressure head, diffusion due to a concentration gradient, capillary suction due to surface tension acting in the capillaries, or adsorption-desorption phenomena, involving fixation and liberation of molecules on the solid surface due to mass forces, may act simultaneously within the drying material (Kropp *et al.*, 1995). Evaporation and condensation within the porous solid is also important for determining the phase in which moisture is transported through the material (Andrade *et al.*, 1999; Mainguy *et al.*, 2001). As stated above, all these phenomena may act simultaneously and be predominant in different regions of the cement paste (aggregates are usually considered to be impervious, with the exception of lightweight concrete). A detailed description of these mechanisms is out of the scope of this thesis and may be found elsewhere, together with an experimental study of the determination of transport properties for modeling purposes (Baroghel-Bouny, 2007 Part II).

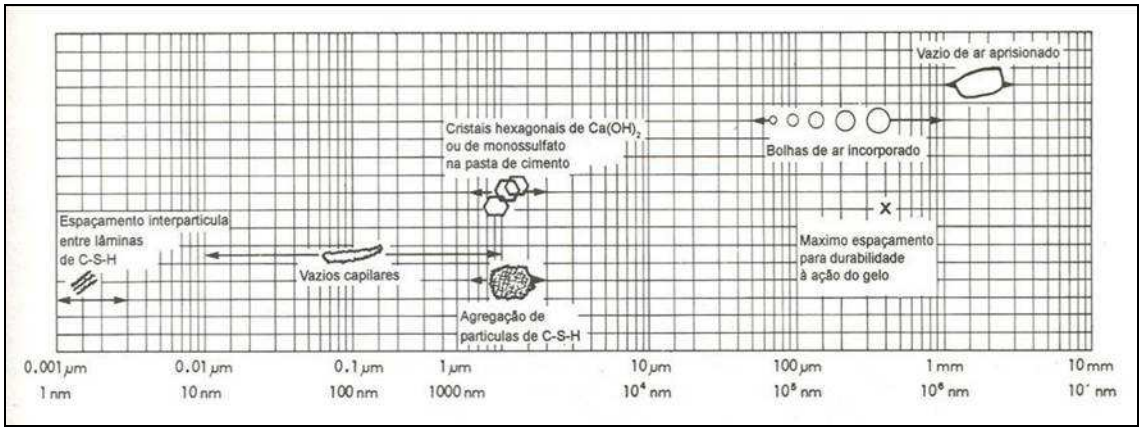

Figure 3.2. Typical size range of pores and hydration products in a hardened cement paste (from Mehta & Monteiro, 2006).

Different mechanisms for explaining the observed volumetric changes of concrete during drying have been proposed over the years. It is now accepted that in fact the observed behavior is a result of the interaction of all these mechanisms, each of those acting predominantly in a predetermined internal relative humidity range. They will be briefly described below as they represent the fundamental aspects behind macroscopic

observations. A detailed description may be found elsewhere (Hansen, 1987; Bazant, 1988; Scherer, 1990; Soroka, 1993; Kovler & Zhutovsky, 2006). Although originally proposed for cement paste, their applicability for concrete or mortar is also valid because the aggregates do not affect the shrinkage mechanism as such, but rather exert a restriction to shrinkage, thus provoking only a quantitative change of shrinkage strains.

Capillary tension

This is probably the most well documented phenomenon in drying porous media. In summary, a meniscus is formed in the capillaries of the hardened cement paste (HCP) (capillary pores) when it is subjected to drying, causing tensile stresses in the capillary water (due to surface tension forces). In turn, these tensile stresses are balanced by compressive ones in the surrounding solid, bringing about elastic shrinkage strains (see figure 3.3a). This mechanism is supposed to act in the high RH range (until approximately 50% RH), since it fails to explain shrinkage deformations at low RH (with the use of the well-known Kelvin equation it can be seen that the maximum hydrostatic stress is reached at 40 to 50% RH). Indeed, it predicts the recovery of shrinkage strains at an advanced stage of the drying process. The Kelvin equation reads

$$ln(\mathrm{H}) = \frac{M_v}{\mathrm{RT}}\gamma\left(\frac{1}{\mathrm{r}_1}+\frac{1}{\mathrm{r}_2}\right) \tag{3.1}$$

in which H = RH, γ= surface tension force, r_1 and r_2 = radii of the meniscus (r_1=r_2 for a cylindrical pore), T = temperature, M_V = molar volume of water and R is the universal gas constant. It represents the drop in RH required to support a meniscus in the pore of radii r_1 and r_2 (see e.g. Bazant, 1988). In turn, the force exerted on the pore walls (σ) may be calculated by the Laplace equation as follows

$$\sigma = \gamma\left(\frac{1}{\mathrm{r}_1}+\frac{1}{\mathrm{r}_2}\right) \tag{3.2}$$

Surface tension

Molecules within a solid material are in equilibrium due to the attraction and repulsion forces in all directions from neighboring molecules. In the case of molecules lying on the surface of the material, due to lack of symmetry, there is a resultant force perpendicular to the surface that provokes its contraction, behaving like a stretched elastic skin (see figure 3.3b, from Soroka, 1993). The resulting tension in this surface is often been referred to as *surface tension*. This force induces compressive stresses in the material, which in turn suffer elastic deformations. This volume reduction may be non-negligible in the case of cement gel particles (having large surface to volume ratios). This phenomenon is highly affected by the moisture content and more specifically by the adsorbed water layers on the surface of the material. When an adsorbed water layer is present, a decrease of the compressive stresses mentioned above will be effective, thus decreasing also the surface tension. Accordingly, a volume increase or swelling will take place. In a similar way, when drying occurs this layer may eventually disappear, causing a volume reduction or shrinkage due to the increase in surface tension. It has been suggested that this mechanism is only valid in the low RH regime, with values of up to 40% RH (Wittmann, 1968).

Disjoining pressure

The thickness of the adsorbed water layer mentioned above is determined, at fixed temperature, by the local RH (an increase in this last one produces an increase in the

thickness). In the case that different surfaces are very close to each other within the material, these layers may not be able to fully develop under the surrounding RH, thus forming zones called areas of hindered adsorption, where disjoining (swelling) pressures develop (figure 3.3c). This pressure tends to separate the two surfaces causing swelling of the material. Accordingly, in the opposite case (i.e. when drying occurs) these pressures decrease and adjacent particles separation diminish so that shrinkage strains take place. This mechanism was proposed in the 60's by Powers in order to explain the continued shrinkage below 40% RH and has been recently recognized to be the dominant mechanism behind hygral expansion above 50% RH, since the pore solution at the nano-scale cannot form a capillary meniscus (Beltzung & Wittmann, 2005).

Movement of interlayer water

This mechanism is attributed to the layered-structure of the calcium silicate hydrates (CSH) within the cement gel (Bazant, 1988; Jennings, 2008). When RH drops to about 10%, it is generally agreed that interlayer water (figure 3.3d) may migrate out of the CSH sheets, thus reducing the distance between these layers and causing macroscopic shrinkage strains. It should be noted that a small amount of water loss in this range gives rise to large volume reductions.

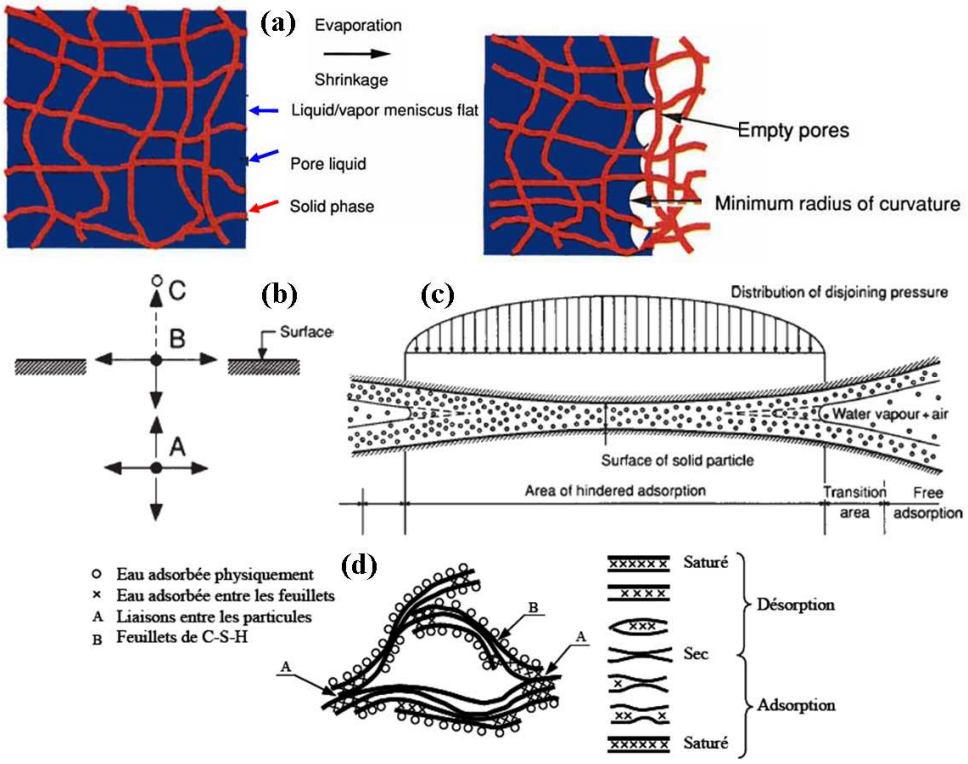

Figure 3.3. Schematic representations of different mechanisms acting on drying of concrete. (a) Capillary effects on HCP, such as shrinkage and meniscus formation (from Scherer, 1990). (b) Surface tension forces, showing an equilibrated molecule A inside the material and a molecule B on the surface exerting a compressive stress on the solid (from Soroka, 1993). (c) Hindered adsorption area and the development of disjoining pressures (from Soroka, 1993). (d) CSH gel microstructure model proposed by Feldman and Sereda, showing different states of water, including adsorbed water between sheets susceptible to escape at very low RH (from Benboudjema, 2002).

As a result of the interaction between the above mentioned mechanisms (each one acting predominantly within a specific RH range), and the 'structural effect' as a consequence of crack formation, the relation between the observed shrinkage strains and the moisture losses show a highly nonlinear behavior, with points of discontinuity. This is shown in figure 3.4, in which typical curves of shrinkage vs. moisture losses for small specimens, constructed with a large RH range, are presented (see also Jennings *et al.*, 2007). Accordingly, it can be observed that the loss of free water at the first stages of drying causes little shrinkage strains, while this tendency reverts at more advanced drying stages. Several researchers have tried to relate these kinks in the curves with the different mechanisms acting at different ranges (Bazant, 1988; Han & Lytton, 1995; Kovler & Zhutovsky, 2006). Although this procedure seems valid, the quantification of the influence of each of these mechanisms is extremely difficult, reason by which the reconstruction of shrinkage vs. moisture loss curves by this procedure is far from being usual practice. Moreover, the inability to completely avoid crack formation due to ever existing hygral gradients make even more difficult this task, as the measured shrinkage strains are reduced due to skin microcracking (Thelandersson *et al.*, 1988; Wittmann, 2001). For example, it was found that cement paste specimens with a thickness varying between 1 and 3mm showed surface microcracking when subjected to drying, although it was suggested that these microcracks did not affect the shrinkage strains (Hwang & Young, 1984).

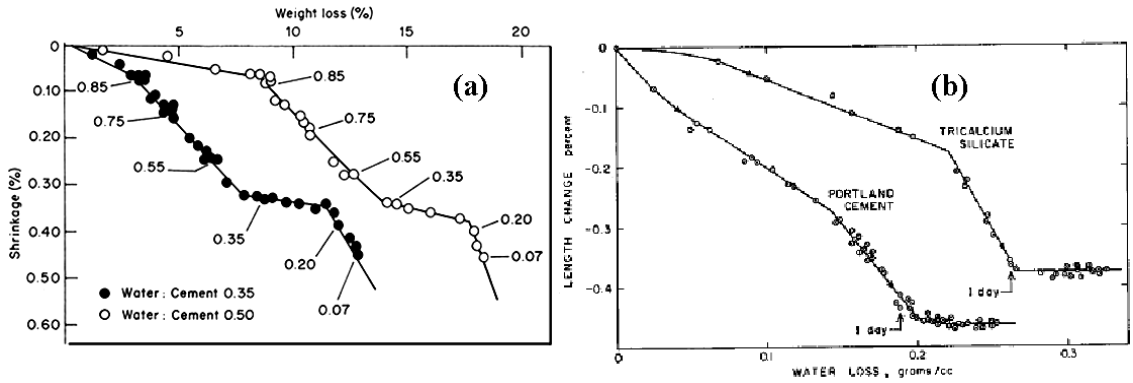

Figure 3.4. Typical drying shrinkage vs. water loss curves: (a) for different w/c ratios, highlighting measured RH at each point during the drying process of a HCP (data by Roper, 1966; taken from Bazant, 1988); (b) for different HCP slabs (15x80mm and thicknesses between 1-3mm), drying at 47% RH (from Helmuth & Turk, 1967).

3.1.2 Factors affecting drying shrinkage

The factors affecting drying and shrinkage in concrete are well-known and treated in various text books (see e.g. Soroka, 1993; Mehta & Monteiro, 2006; Neville, 2002). For this reason they will only be briefly discussed in this section. They are often interrelated, although they can be grouped into two main categories. On one hand, the environmental factors will set up the external conditions, such as humidity level, ambient temperature or wind velocity. The second group involves the characteristic (intrinsic) properties of the concrete material, as may be the aggregate content and their properties, the w/c ratio, the water content and the cement content. The curing and storage conditions are somewhere in the middle of the previous classification, since they consist of the often controlled external conditions which will to a great extent define the quality of the material, i.e. its characteristic properties. Also the influence of additives can be important in some cases, although this is out of the scope of this thesis.

a) Environmental conditions

The environmental conditions will define the severity of the drying process, being more detrimental when there is a combination of dry conditions (low RH), elevated temperatures and a high wind velocity. A low ambient RH will produce strong gradients near the drying surface, thus increasing the drying rate (figure 3.5). The effects of wind velocity and temperature are smaller than that of RH and their consideration is more important for determining the early age shrinkage strains (e.g. plastic shrinkage).

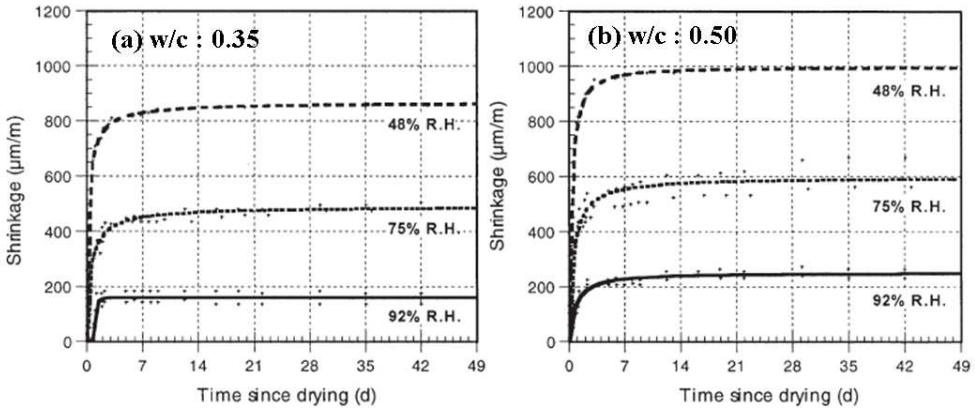

Figure 3.5. Effect of ambient (constant) relative humidity of exposure on the drying shrinkage rate for 4x8x32mm mortar specimens with two different w/c ratios (a) 0.35 (b) 0.50 (from Bissonnette *et al.*, 1999).

b) Aggregate concentration and stiffness

The presence of aggregates in concrete restrict the overall deformations, as regular aggregates do not generally show appreciable creep when subjected to stresses, nor they are subjected to drying due to the low permeability as opposed to the cement paste. Table 1 shows the influence of aggregate content on drying shrinkage (data from Neville, 2002). It can be clearly noticed that the higher the aggregate/cement ratio, the lower the shrinkage strains, due to the mentioned restraining effect, but most of all because the shrinking volume fraction of the composite material (concrete) decreases.

aggr./cem.	**Shrinkage at 6 months ($x10^{-6}$) for w/c ratio of:**			
Ratio	**0,4**	**0,5**	**0,6**	**0,7**
3	**800**	**1200**	**----**	**----**
4	**550**	**850**	**1050**	**----**
5	**400**	**600**	**750**	**850**
6	**300**	**400**	**550**	**650**
7	**200**	**300**	**400**	**500**

Table 1. Typical values of shrinkage strains in mortar and concrete samples with a squared cross section of 127mm^2, exposed to a 50% RH environment at 21ºC (from Neville, 2002).

Thus, the ratio of the shrinkage of concrete (C) to the shrinkage of HCP depends on the aggregate volume fraction (a). This can be expressed as follows

$$\frac{S_C}{S_{hcp}} = (1-a)^n \tag{3.3}$$

where the exponent n is typically between 1.2 and 1.7 (Neville, 2002). This relation is plotted and contrasted to experimental results in figure 3.6a, for n = 1.7. The size and/or grading of the aggregate fraction do not have an effect on the shrinkage of concrete, provided the cement paste is the same. Nevertheless, more internal microcracking is to be expected in the case of larger aggregates, due to an increase in the restraining effect (Bisschop & van Mier, 2002), which is not considered in equation 3.3.

The stiffness of the aggregates has also important consequences on shrinkage, since the restraining effect highly depends on this parameter. As a general rule it can be stated that the lower the stiffness of the aggregate the higher the shrinkage strains (to illustrate, in the limiting case, when this rigidity would tend to zero the aggregates would perform as macropores or holes, i.e. with no restraining effect at all, thus showing clearly the maximum extent of this effect). The elastic modulus of the aggregates obviously affects that of the concrete material, for example when comparing normal and lightweight concrete made with the same cement paste. In figure 3.6b the effect of the stiffness of the aggregates on the shrinkage strains is shown in terms of the secant modulus of the concrete. However, it should be noted that in the case of lightweight concrete, the drying process is rather different, as water may diffuse through aggregates and migrate out of them (since they are much more porous than normal aggregates), which may in turn crack due to hygral gradients (Lura & Bisschop, 2004). It should be noticed that equation 3.3 is able to approximately capture the effect of aggregate rigidity by fitting the exponent n, which should depend on the elastic properties of the aggregates.

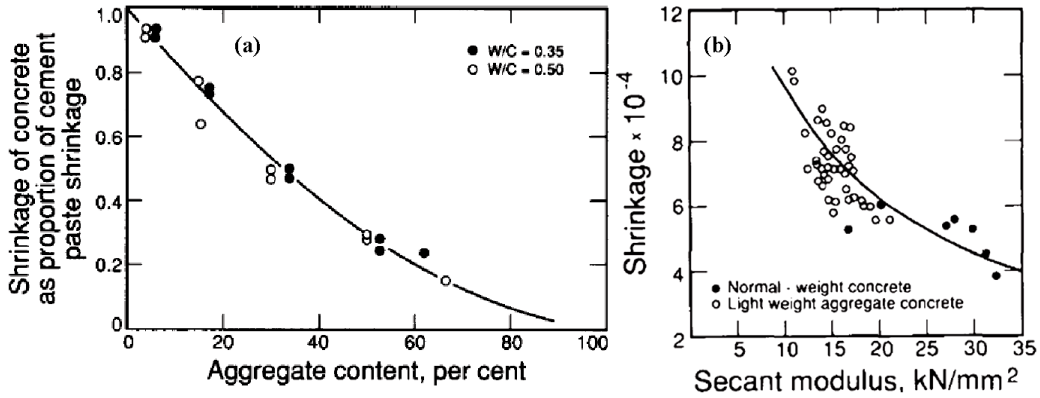

Figure 3.6. (a) Effect of aggregate concentration on shrinkage of concrete: theoretical curve predicted with equation 3.3 and n = 1.7 vs. experimental results by Pickett (from Soroka, 1993). (b) Relation between shrinkage strains and concrete secant modulus of elasticity, data by Richard (from Soroka, 1993).

c) Water to cement ratio (w/c), water content and cement content

The w/c ratio and the contents of water and cement are three interrelated factors, since by fixing any pair of them the third one can be immediately determined. Starting with the effect of the concentration of these two components (water and cement), it can be shown that the greater the concentration, the greater the shrinkage deformations. In the case of water, increasing its content will lead to increasing the amount of evaporable water, and thus the potentiality to suffer shrinkage strains. On the other hand, the cement content determines the fraction of cement paste in concrete. Obviously, shrinkage will be greater the higher the cement paste content, which represents the shrinking phase of the material (since aggregates are generally inert).

The w/c ratio determines how much water there is in the cement paste. It is often used to empirically determine concrete strength and other properties of concrete, since it gives a measure of the HCP quality, i.e. the porosity will be higher (and thus its durability will be poor and the strength will be lower) as this ratio increases its value. Accordingly, reducing the w/c ratio will lead to a considerable decrease in the shrinkage strains and the porosity of the cement paste. This is shown in figures 3.5 and 3.7, where shrinkage strains for mortars and concretes with different w/c ratios are compared. In practice, it is usually the requirements of mixture workability and durability of concrete that determine the water content and the w/c ratio, respectively, thus automatically fixing the cement content, although this is not always the case.

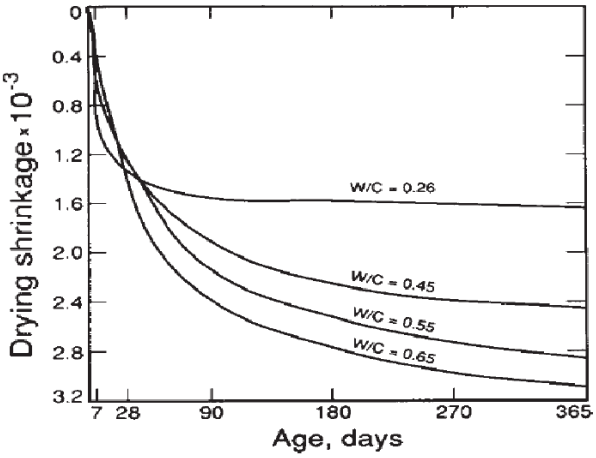

Figure 3.7. Effect of w/c ratio on the drying shrinkage of concrete as a function of time, data by Haller (from Soroka, 1993).

d) Addition of admixtures

The effect of mineral admixtures on the shrinkage strains and mechanisms is diverse. Their addition produces changes in the microstructure of the cement paste, as well as modifications of the pore structure. It is not the intention of this study to describe these issues. In this thesis, only ordinary Portland cements (OPC) will be studied. The avid reader is referred to concrete textbooks (Soroka, 1993; Mehta & Monteiro, 2006) and more specific literature on the subject (Roncero, 1999; Kovler & Zhutovsky, 2006).

3.1.3. Sorption/desorption isotherms

The so-called water vapor sorption-desorption isotherms relate the mass water content of the hardened cementitious material at hygral equilibrium, with RH, at a constant temperature. In order to determine these curves, water vapor desorption-adsorption experiments must be performed, in which each point in the curve is obtained when the external RH (measured) is equal to the internal one (i.e. the RH of the gaseous phase of the pore network), since the material must be at thermodynamic equilibrium with the surrounding environment. This relation is a key feature of drying models, since almost always there is the need to relate these variables at some point in the analysis (see section 3.4.3), unless the experimental determination of the different parameters involved is fully performed in terms of the RH (as proposed in Ayano & Wittmann, 2002). A recent work by Baroghel Bouny (2007) discusses in detail the experimental procedure to determine these curves, the relevant factors affecting this equilibrium, like the w/c ratio (figure 3.8b), the predominant transport mechanisms acting on different RH ranges, and presents the results of a large experimental campaign. One important

conclusion of that work is the fact that the aggregate content do not have any effect on the resulting desorption isotherms, as shown in figure 3.8a, thus allowing to employ desorption isotherms determined on concretes for the behavior of the matrix (assuming the aggregates as impervious) in a meso-scale simulation, as in this thesis. This finding is suggested to be due to the fact that the void size range, where the moisture equilibrium processes described by the isotherms take place, is much smaller than the paste-aggregate interface heterogeneities and the typical voids present in this zone. Therefore, the micro and meso-pore ranges investigated by sorption processes, are identical for concrete and HCP (Baroghel Bouny, 2007).

The desorption isotherms are mainly dependent on the pore structure of the HCP. Thus, any factor affecting this structure will have a non-negligible influence on the shape of these equilibrium curves. Among these factors, the most relevant are the w/c ratio (figure 3.8b), the curing time, the type of cement (and obviously the addition of admixtures) and the temperature (Xi *et al.*, 1994a). The drying and wetting cyclic behavior generally shows a considerable hysteresis (see figure 3.8a) which is probably due to the liquid-solid interaction (Pel, 1995; Baroghel-Bouny, 1999; Baroghel-Bouny, 2007). If focus is made on the drying process, as in this thesis, this fact is not relevant, and therefore one can assume in practice a univocal relation between RH and moisture content (except in the cases where the desorption isotherm is very steep near saturation, as with poor concretes with high w/c ratios, see Nilsson, 1994 or Baroghel Bouny, 2007). This is not the case for a thermo-hygric analysis (e.g. in natural weathering conditions), since there may be more than one possible value of w_e for each value of the RH, turning the use of desorption curves in these cases a delicate matter (Andrade *et al.*, 1999).

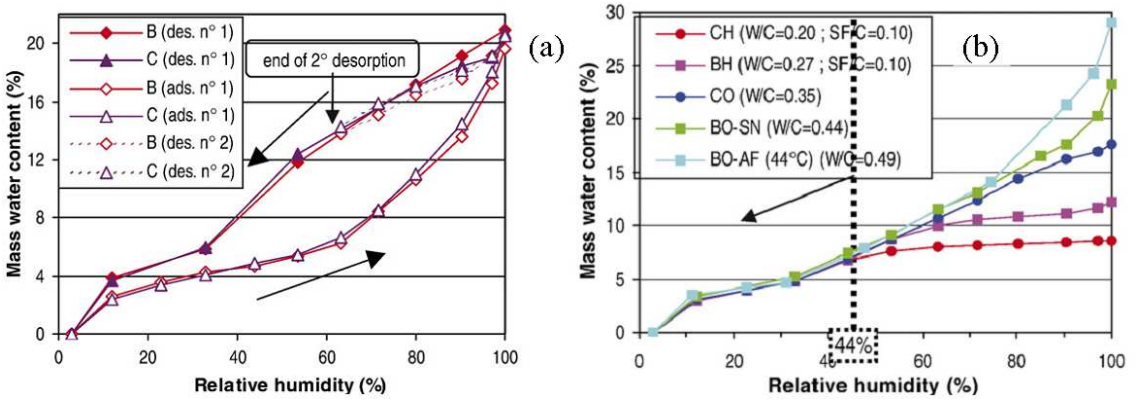

Figure 3.8. Typical sorption-desorption isotherms experimentally obtained: (a) showing the negligible difference between sorption-desorption isotherms obtained for concrete slices (B) and HCP crushed specimens (C); (b) showing the effect of w/c ratio on the shape of the curves (from Baroghel-Bouny, 2007).

It is interesting to note that the sorption-desorption isotherms are equivalent to the well-known water retention curves, mostly used in geotechnical engineering, which relate the capillary pressure (p_c) at a point with the degree of liquid water saturation (S_l). This equivalence may be verified by introducing the following relations:

$$p_c(H) = \rho_l \frac{RT}{M_v} ln(H) \tag{3.4}$$

$$w_e = S_l \cdot \phi \cdot \rho_l \tag{3.5}$$

in which ρ_l is the liquid density, R the gas constant, T the temperature (K), M_v represents the vapor molar mass, ϕ is the porosity and w_e is the evaporable water content. Equation 3.4 represents the well-known psicrometric law and the second one relates the moisture content with the degree of saturation. Figure 3.9 shows this transformation, corresponding to the expression proposed by Norling (1994) for the desorption isotherms (see Chapter 4 for details on the formulation). In this way, recent studies have used water retention curves common to soil mechanics, like the van Genuchten curve, for studying drying of concrete (Savage & Janssen, 1997; Mainguy *et al.*, 2001).

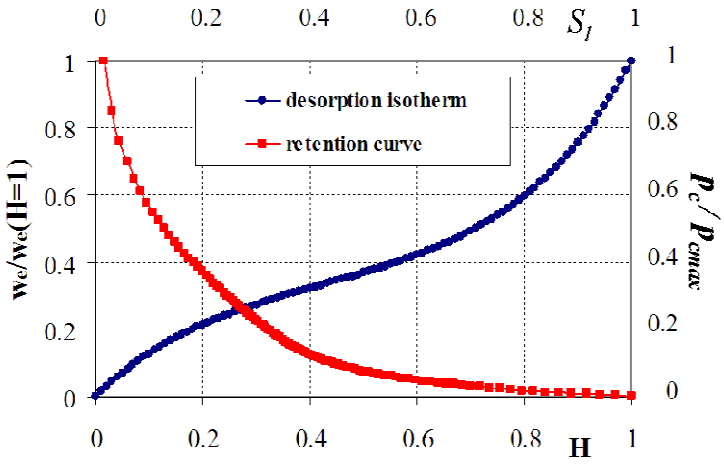

Figure 3.9. Comparison between desorption isotherm given by the expression proposed by Norling (1994) and equivalent water retention curve.

3.1.4. Measuring shrinkage strains

A brief reference should be made to some practical aspects of shrinkage strain measurements in concrete specimens, as another important factor when analyzing shrinkage tests. The position of the points of measurement of the (longitudinal) shrinkage strains plays an important role in the determination of the coupled hygro-mechanical behavior of concrete (figure 3.10). Due to the fact that drying is a diffusion process, internal RH will not in general be at equilibrium with the environment. Thus, nonlinear shrinkage strains distributions within the thickness of a concrete sample will develop (as shown in figure 3.11). It has been experimentally confirmed that deformations measured at the surface of the samples are larger than those measured at the centre of the specimen, as can be observed in figure 3.10b (Wittmann, 1993). The effect of skin microcracking due to hygral gradients will also alter the deformations of the outer layers, reducing the longitudinal strains (see next section). The slenderness of the samples is also of great importance, since the end effects will alter the moisture distribution (in the case of unsealed conditions), and most importantly the Saint-Venant's principle will not be fulfilled, i.e. plane sections near to the specimen ends will not remain planar as the specimen deforms (Acker & Ulm, 2001). This is the main reason to use slender specimens for drying shrinkage tests and to perform the measurement of longitudinal strains far from the sample ends (approximately at 1.5 times the diameter or edge of the specimen, as a general rule). In this regard, figure 3.10b shows the decrease in shrinkage strain as a function of the height of the concrete samples (for constant diameter).

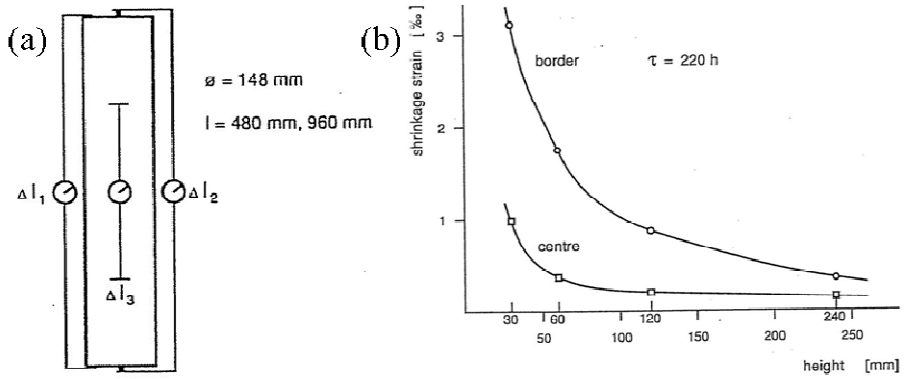

Figure 3.10. (a) Different possibilities of strain measurement in a drying shrinkage test. (b) Relation between the height of concrete specimens of constant diameter and the measured longitudinal strains at the border and at the centre of the samples (from Wittmann, 1993).

3.1.5. Shrinkage-induced microcracking and its detrimental effects

During the drying process, whether it is due to internal or external restrictions, self-equilibrated stresses are usually generated within a specimen cross-section. The moisture gradients are responsible for a differential drying (and thus shrinkage) of the specimen, causing tensile stresses near the exposed surface and compressive stresses in the inner layers (due to compatibility of strains and equilibrium considerations), as can be seen in figure 3.7 (Bazant, 1988). When the induced-tensile stresses exceed the tensile strength of concrete (which is an age-dependent property) cracking will irremediably occur. At the beginning of drying, microcracks will mainly develop perpendicular to the drying surface. In this thesis, we will call microcracks all cracks with a width smaller to 50 microns, which is typically the maximum crack opening for drying shrinkage induced cracks, in accordance with Shiotani *et al.* (2003). It should be noticed that a RILEM state-of-the-art report on microcracking suggests that this limit should be 10 microns (Damgaard & Chatterji, 1996), although this definition is somewhat arbitrary. These microcracks may potentially induce a higher drying rate, increasing the effective diffusivity of the material, and thus favoring a higher degree of microcracking, indicating that it is a coupled process, i.e. that there is a feedback of the drying-induced microcracking on the drying process itself. Upon rewetting, microcracks may partially or fully close due to swelling of the material (Kjellsen & Jennings, 1996).

3.1.5.1. Coupling between drying-induced microcracks and drying process

The influence that the drying-induced microcracks have on the drying process and the effective transport properties of the material is still an open matter. In fact, even the effect on drying of the macrocracks due to mechanical loading is controversial. Most of the experimental data corroborates the intuitive idea that a crack represents a preferential pathway for moisture to escape the material, and thus that a cracked material should dry faster than an uncracked one. Larger discrepancies are found when quantifying this effect. This may be due to the intricate crack morphology, the high sensitivity to crack opening and roughness of the crack surfaces (Carmeliet *et al*., 2004), the connectivity of the crack network and, in the case of mechanically-induced cracks, the difficulty added by the typical bridging and branching effects of the crack patterns in concrete. In the case of drying-induced microcracks, our inability to perform tests where microcracking is avoided, which is needed as a reference test for comparison, represents an additional difficulty. Some authors have tried to avoid it by preparing small samples,

in the mm range, arguing that the moisture gradients in this case are very small (Hwang & Young, 1984). In the analytical field, it will be shown in the next section that current theoretical tools may be insufficient to perform a rigorous quantitative study. At present, it is not possible to evaluate the diffusivity of one single microcrack, or the critical crack opening beyond which the drying process is unaffected by its presence, although in recent years a lot of progress in the experimental field has been made (Beyea *et al.*, 2003; Carmeliet *et al.*, 2004). Some recent studies have focus on the effect of cracks on the air gas flow (dry air + water vapor) and tried to correlate data with analytical formulas in terms of crack opening, showing encouraging results (Ismail *et al.*, 2006).

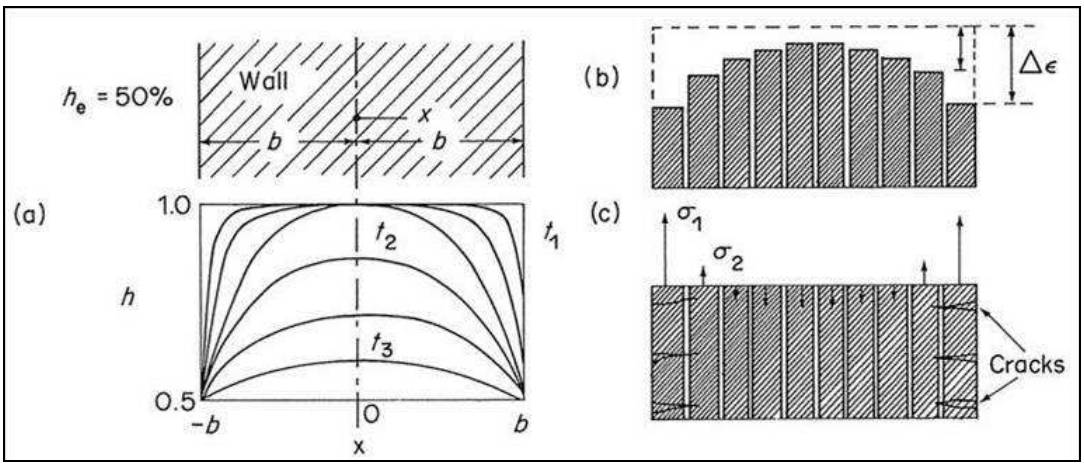

Figure 3.11. Concrete wall exposed to drying: (a) Geometry and RH distribution at different drying times; (b) corresponding shrinkage strains for each layer, as if they were not subjected to any kind of restriction; (c) induced-stresses and cracking due to restoration of compatibility conditions (from Bazant, 1988).

Bazant and coworkers (Bazant *et al.*, 1987) performed drying experiments on C-shaped reinforced concrete specimens with and without mechanically-induced cracks, perpendicular to the drying surface (due to the presence of reinforcement they managed to produce constant width and regularly separated macrocracks). They concluded that cracks with an opening of 100 microns or greater significantly influence the drying process (see figure 3.12a). However, they neglected the influence of microcracking due to drying exclusively, so that the results only show the increase due to mechanically-induced cracking.

Wittmann studied drying of concrete cylinders of constant diameter (80mm) and different heights (20mm and 320mm), with the underlying assumption that drying does not provoke significant microcracking in the short specimens because drying-induced stresses are strongly reduced due to the curvature of the end faces (Wittmann, 1995). On the other hand, in the central portion of the larger specimens the hygral stresses are fully developed. By measuring the weight losses as a function of time, he fitted this experimental data with a non-linear diffusion equation in order to find the dependence of the diffusion coefficient on the moisture content in both cases, which is shown in figure 3.12b. He concluded that the influence of microcracking on the rate of drying is small and that drying of concrete can be studied in an uncoupled way.

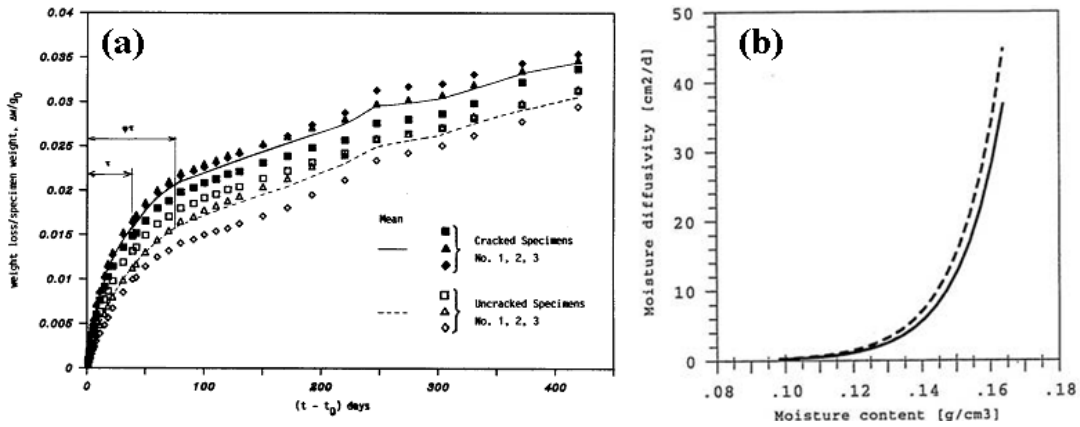

Figure 3.12. Experimental results showing the influence of cracks on drying process: (a) weight loss vs. time for mechanically cracked and uncracked C-shaped concrete specimens (from Bazant *et al.*, 1987); (b) moisture diffusion coefficient (obtained by fitting moisture loss vs. time experimental curves) vs. moisture content, the dashed line indicating a slight increase due to drying-induced damage (from Wittmann, 1995).

Gérard and coworkers designed a special test apparatus for studying the permeability of concrete, previously subjected to tensile stresses, in order to assess the effect of homogeneous damage and/or single macrocracks on the transport properties (Gérard *et al.*, 1996), by performing permeation tests. They found increments in permeability of up to 100 times the sound concrete value. This notorious increase is explained by the nature of the tensile-induced damage, and by the fact that permeability tests where carried out perpendicular to the loading direction. Other researchers studied the permeability of concrete under compressive stresses and concluded that relatively small increases in permeability are obtained even when loading to levels of up to 75% of the peak or higher (see e.g. Samaha & Hover, 1992). The effect of a main crack, mechanically-induced by the tensile splitting test, on permeability of concrete was evaluated by Shah and coworkers (Aldea *et al.*, 1999). They found the permeability coefficient to be very sensitive to changes in the crack opening, ranging from 50 to 350 microns, with a three fold increase when passing from sound concrete to a specimen with a 350 microns traversing crack.

Hearn (1999) performed experimental tests to determine the different nature of the effect of drying-induced and loaded-induced (under compression) cracking on the permeability of concrete. The insensitivity of water permeability (tested after unloading) to the compressive load-induced cracking was confirmed, even for load levels as high as 80% of the compressive strength. It was suggested that this is due to the discontinuous nature of the crack system and to partial closing at unloading. On the other hand, the permeability was significantly increased (and said to be isotropic) due to the presence of drying-induced microcracks, although drying was achieved by oven-drying the samples at 105ºC, which is not representative of real environmental conditions and probably alters the internal structure of the HCP.

An interesting study of the superficial microcracking quantification of high strength concrete due to combined drying shrinkage and creep tests underlined the sensitivity of the resulting crack patterns to compressive loads (Sicard *et al.*, 1992). With the use of the replica technique (which allows the analysis on loaded samples), a scanning electron microscope (SEM) and digitizing the images obtained in this way from the exposed external surface of the specimens, they were able to map the anisotropy of the crack pattern. The total projected length in a given direction is transferred onto a polar

reference plane in order to construct the "rosette" (or polar) maps, showing the preferential direction of the cracks. This is shown in figure 3.13, presenting their results for drying shrinkage microcracking on unloaded specimens, and for cracking in a creep test with a load of 32MPa, both for the loaded specimen as well as on unloading of the same sample. It can be clearly seen in the rosette diagram that drying shrinkage microcracking is almost isotropic in the surface, and that the addition of a high compressive load prevents horizontal cracks (assuming vertical load) to form, thus resulting in a highly anisotropic rosette. On unloading, the tensile stresses due to drying near the surface develop again and shrinkage microcracking can be observed, showing a more homogeneous rosette than in the case of the loaded specimen.

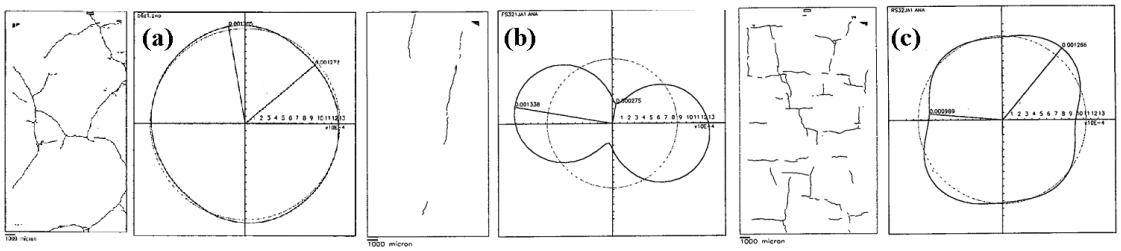

Figure 3.13. Crack patterns and rose diagrams of the specimen's surfaces exposed to drying of different samples: (a) drying shrinkage microcracking on unloaded specimens; (b) creep test with a load of 32MPa for the case of loaded specimen; (c) creep test on unloading of the same sample (adapted from Sicard *et al.*, 1992).

3.1.5.2. Effect of the aggregates on drying shrinkage microcracking

As the drying process progresses, shrinkage strains translate to the interior of the material. In the case of concrete, which is a highly heterogeneous material consisting of a shrinking matrix surrounding more rigid non-shrinking aggregate inclusions, the differential shrinkage between cement paste and aggregates induce a stress field. This has been studied experimentally and analytically already in the 1960's for different kind of composites, such as plastic specimens with glass inclusions (Daniel & Durelli, 1962), plasticized epoxy with unplasticized epoxy as inclusions (Koufopoulos & Theocaris, 1969), and artificial concrete (Hsu, 1963; Mc Creath *et al.*, 1969). Hsu identified typical crack patterns in cementitious materials using a model concrete material with a square array of sandstone discs as aggregates. In these tests, bond cracks between cement paste and aggregates as well as radial cracks between aggregates where produced by drying shrinkage-induced tensile stresses (figure 3.14a). A few years later, Mc Creath published similar results (figure 3.14b) and stated that "shrinkage shear strains...frequently caused shrinkage cracks to occur along the shortest line between any two particle centres". He also suggested that "the restraining influence of strong, hard aggregate particles induces shrinkage cracks in unloaded specimens and such cracking is more likely in concretes containing high volume fractions of aggregate". These assumptions were later confirmed by many researchers (Chatterji, 1982; Hearn, 1999; Dela & Stang, 2000).

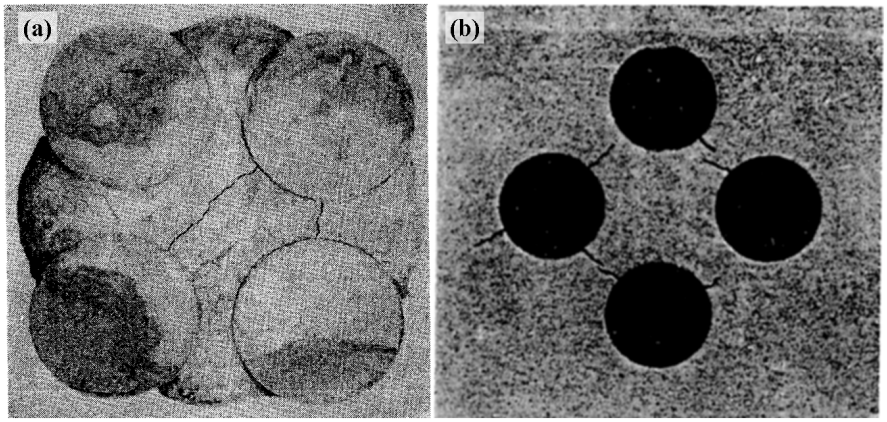

Figure 3.14. Crack patterns of shrinkage tests by (a) Hsu: the specimen consisted of a square array of 4 sandstone discs (distance between discs of 0.4 times their radius) surrounded by cement paste and allowed to dry in air, inducing a certain shrinkage. Bond cracks as well as radial cracks between aggregates are clearly observed (from Hsu, 1963); (b) Mc Creath: shrinkage cracking in a plate model with 13.4% aggregate content, showing radial cracking between aggregates (from Mc Creath *et al.*, 1969).

A recent experimental campaign at Delft University has quantitatively assessed the effect of the aggregate volume fraction and aggregate size on the drying shrinkage induced microcracking in different composites (Bisschop, 2002; Bisschop & van Mier, 2002b), considering a cement paste matrix with mono-sized glass spheres and also regular rounded aggregates. In accordance with previous observations, they identified radial and bond microcracks emanating from large aggregate particles, through the use of more modern techniques, as can be observed in figure 3.15 (see Bisschop & van Mier, 2002a and Shiotani *et al.*, 2003). Moreover, they found that the degree of the aggregate restrain effect on shrinkage and microcracking is greater, the larger the size of the particles and the greater their volume fraction, as will be shown in Chapter 4. The same authors analyzed the effect of drying-induced microcracking of the above-mentioned composites on the drying rate of the specimens (Bisschop & van Mier, 2008). It was determined that the maximum increase due to microcracking was of the order of 10% (as compared to the specimen that showed less microcracking) in specimens with larger aggregates and at a high degree of internal damage (i.e. the worst case scenario). However, this is expected not to be the case in standard concrete materials due to their different compositions, thus concluding that the feedback of these microcracks on the drying rate can be neglected.

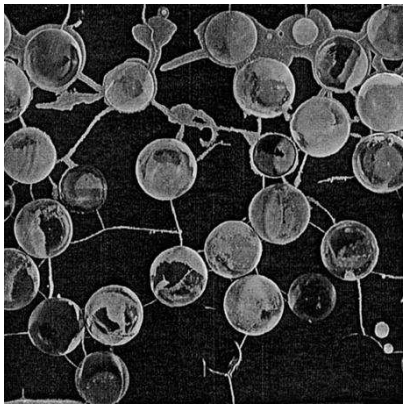

Figure 3.15. Micrograph of cementitious material with glass spherical inclusions with a diameter of 6mm (volume fraction of 50%) and exposed to 20% RH and T=30ºC, corresponding to a stage of 20% of initial water loss. Radial microcracking to the aggregates is clearly observed, as well as cracks perpendicular to the drying (upper) surface (from Bisschop & van Mier, 2002a).

The effect of large aggregates on microcracking due to a shrinking matrix has also been studied analytically (Goltermann, 1994; Goltermann, 1995), assuming an idealized configuration of one single circular aggregate surrounded by an infinite medium. Their results confirmed the appearance of (wide) cracks radiating from the aggregates as well as (thin and tangential) bond cracks between inclusions and matrix. He stated that fracture mechanics predicts that particles below a lower critical size will not cause crack propagation (even if the tensile strength is exceeded), and that this is due to the fact that the energy released for a crack propagating from a particle of radius R will be proportional to R^3, whereas the necessary fracture energy will be proportional to R^2. A few years later, the same study was conducted with the addition of a shell around the spherical aggregate, in order to consider the interface properties on the mechanical behavior (Garboczi, 1997), although only the cases of matrix or aggregate expansion (and not shrinkage) were mainly analyzed (it was analytically determined that a gap between matrix and aggregate is formed due to expansion of the former, result which is useful for the case of sulfate attack, as will be seen in Chapter 6).

3.1.5.3. Effect of drying-induced microcracking on the mechanical properties of concrete

Another important aspect of the drying-induced microcracking is the possible effect on the mechanical properties of concrete (Wittmann, 1973). It has been shown experimentally that excessive drying may cause a reduction of the Young modulus and of the Poisson's ratio of up to 15% and 25%, respectively (see figure 3.16 from Burlion *et al.*, 2005, and Yurtdas *et al.*, 2004; Yurtdas *et al.*, 2005). The drying-related factors that have an influence on the mechanical response have been discussed elsewhere (Benboudjema, 2002 and references therein).

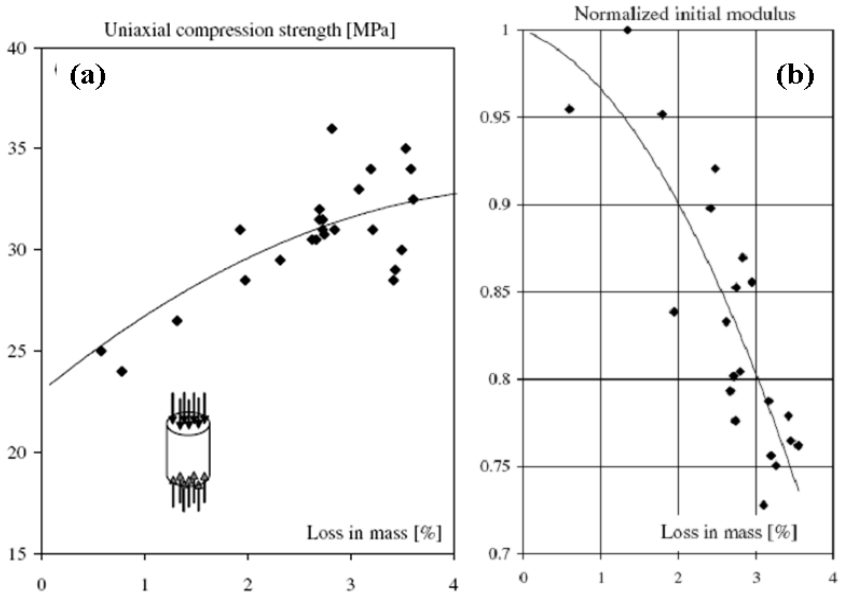

Figure 3.16. Evolution of mechanical properties of concrete cylinders (ϕ = 11cm, h = 22cm; w/c = 0.63; max. aggregate size = 8mm) as a function of water mass loss: (a) uniaxial compressive strength, and (b) normalized elastic modulus (adapted from Burlion *et al.*, 2005).

According to Kanna *et al.* (1998), drying shrinkage affect the mechanical properties of concrete in two ways. On one side, there is an increase in the strength due to an increase in surface energy and bonding between CSH particles. From a geotechnical

point of view, there is an increase in capillary pressure (suction) as saturation decreases, and this pressure acts in the material like an isotropic prestress, leading to a stiffening effect (Pihlajavaara, 1974; Yurtdas *et al.*, 2006). On the other hand, there should be a decrease in stiffness and strength due to microcrack formation. This may explain why experimental studies of the influence of drying on the mechanical properties show dissimilar results and with high levels of scatter (see Yurtdas *et al.*, 2006 and references therein). Most of these experimental studies were based on a uniaxial compression test for evaluating the drying effect. In general, it was found that drying induces an increase in compressive strength (of up to two thirds in mortars with w/c=0.6, as pointed out by Pihlajavaara, 1974), and a decrease in the elastic modulus, as shown in figure 3.16, adapted from Burlion *et al.* (2005).

3.1.5.4. Spacing of superficial drying-induced microcracks

There seems to be a lack of experimental data on the spacing of the superficial drying-induced cracks. In fact, the concept of crack spacing is more related to a two-dimensional idealization of the problem (Bazant & Raftshol, 1982). In reality, surface crack pattern shows polygonal shapes (as in dried clayey soils), so that larger crack spacing would correspond to larger polygons. Crack spacing has been the subject of theoretical and numerical analyses. Bazant and coworkers described the process as follows (see Bazant & Raftshol, 1982 and Ferretti & Bazant, 2006): drying shrinkage in the exposed surface causes a system of equally-spacing parallel cracks; when the parallel cracks get too long compared to their spacing, every other crack closes and the spacing of the remaining (dominant) cracks doubles. With this reasoning, a third system of dominant cracks may develop if shrinkage continues. It was shown that the spacing (s) of the dominant cracks increases on the average as s = 0.69a (a = length of the cracks). This idealization (for a semi-infinite medium) is shown in figure 3.17b. The formation of primary (large number of closely located cracks), secondary (spacing of 2.5cm) and tertiary dominant (with a spacing of 10cm and a maximum opening of 25microns) drying shrinkage cracks was later confirmed with numerical simulations (Granger et al. 1997b). In a further study, an empirical expression for the increased diffusivity due to cracking was proposed as $D_{app} = (1+c^3/s)\cdot D$, where D is the diffusion coefficient for the uncracked material, c the crack width and s the crack spacing (Bazant *et al.*, 1987). This empirical expression shows that an increase in crack spacing yields a decrease in the effective diffusivity of the cracked material. An interesting experimental study, in which crack spacing was analyzed, was performed by Colina and Acker (2000). They considered a microconcrete block of $1m^3$ (w/c = 0.7) drying on two opposite faces, as well as a model material made of sand and clay casted in squared molds with different thicknesses. For the concrete block, they only detected the densification of skin microcracking over time (figure 3.17a). In the case of clay-sand mixtures, they found a correlation between the length of the drying surface side (on square cross-sections) of the specimen and the crack spacing, for given thicknesses. In this way, they proposed a relation between final mean crack spacing and the dimensions of the model material specimens (length of an edge and thickness of the squared specimens). The applicability to cementitious materials was, however, not discussed.

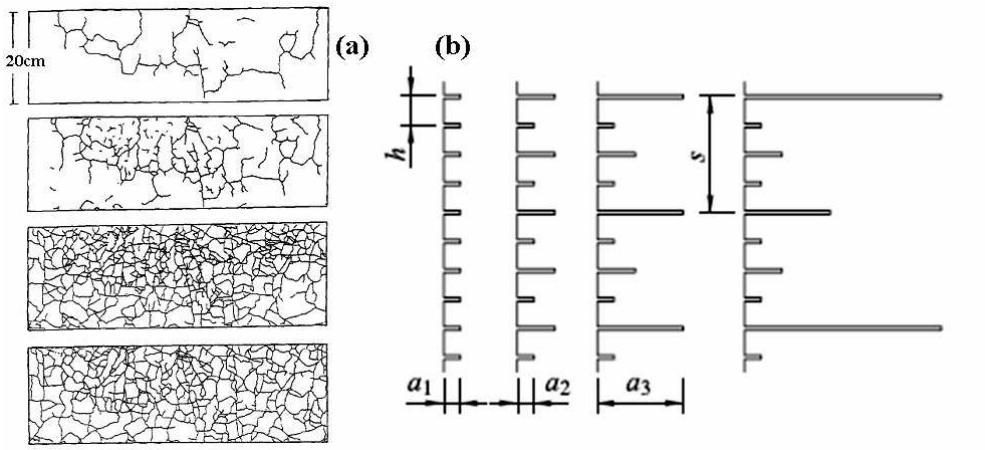

Figure 3.17. (a) Drying-induced microcracking network in microconcrete block (from Colina & Acker, 2000) at different drying times (128, 178, 228 and 588 days from top to bottom); (b) idealization of the evolution of a system of parallel shrinkage cracks and crack spacing as a function of crack length (after Bazant & Raftshol, 1982).

3.1.5.5. Influence of cracking on the transport of ions in cementitious materials

Efforts in quantifying the effect of cracks on the transport of ions are worth to be mentioned, since durability of concrete may be considerably affected by this preferential ways into (or out from, as in the case of leaching) the material for deleterious substances. Many authors have experimentally studied the ingress of ions in cement-based materials, often in the framework of nuclear waste disposal structures (Locoge *et al.*, 1992), in which durability requirements are higher than for regular concrete structures.

Chloride ions have been preferred in the literature due to the fact that this type of attack is the major cause of steel corrosion in reinforced concrete structures (see Djerbi *et al.*, 2008 and references therein). There appears to be no such studies for the case of sulfate ions diffusion. Locoge and coworkers studied diffusion of chlorides through concrete samples subjected to very high hydrostatic pressures of up to 200MPa, inducing different levels of microcracking (Locoge *et al.*, 1992). They concluded that the effective diffusivity of the medium was not significantly affected by microcracking. On the other hand, more recent studies have shown that chloride permeability is greatly affected by microcracks in concrete (Aldea *et al.*, 1999, Djerbi *et al.*, 2008; Ismail *et al.*, 2008). Xi & Nakhi (2005) experimentally studied the effect of mechanically-induced damage on the diffusion of chlorides in concrete hollow cylindrical specimens subjected to compression loading cycles (75% of the peak load) and proposed a composite model to simulate the increase in effective diffusivity of the distressed material. They determined the diffusivity of the damaged phase to be 4 times larger than that of the undamaged material. Cracks are usually generated with a tensile splitting test, thus limiting the lower bound of crack widths to about 30 to 50 microns (Djerbi *et al.*, 2008). This bound may be not enough to study the effect of drying-induced microcracks (or even those provoked by freeze-thaw cycles) on the transport of ions. Nonetheless, results obtained have demonstrated the importance that cracks may have on durability analyses. An alternative way of generating microcracks is subjecting concrete samples to rapid freeze/thaw cycles. With this technique, the rate of chloride migration through 15 mm thick concrete slices was increased by 2.5 to 8 times (Jacobsen *et al.*, 1996). Djerbi and coworkers found that for average crack openings of 80 microns the diffusion through the cracks was the same as in a free solution (Djerbi *et al.*, 2008). For lower

crack openings (from 30 to 80 microns), the diffusivity increased almost linearly with the crack width. Finally, by comparing results of different mixes, they concluded that the roughness of the crack walls had no effect on diffusion through the crack. They suggested that the porosity of the uncracked material has a considerable effect on the transport through the crack.

Recently, experimental tests were performed on doughnut-shaped mortar specimens (5mm thickness, 15mm in diameter and w/c = 0.48) with a mechanical expansive core in the center used to induce controlled cracking with a wide width-range from 6 to 325 microns (Ismail *et al.*, 2008). This test series probably represents one of the most complete studies of diffusion of chloride ions through opened cracks, covering a wide range of crack widths. They obtained results of the effect of crack opening on the penetration depth of chlorides in the direction perpendicular to the crack plane, for two different ages at cracking (28 days and 2 years, in order to account for the self-healing effect, expected to be more pronounced at early ages due to hydration), and for mechanically-induced cracks and saw-cut cracks (for assessing crack roughness effect). The following conclusions were drawn: crack openings of 200 microns or more act as an exposed surface to the free solution; crack openings below 30 microns (which they suggested as the critical crack opening at which there is no more stress transfer, from a direct tensile test) eliminate chloride diffusion through the crack; intermediate crack openings show that there exist a diffusion process along the crack, being more pronounced in the 2 years old samples (these samples are presumed to show no self healing effect at all).

3.2. Experimental evidence: creep of concrete

Creep is generally defined as the time-dependent strain caused by a stress which is applied onto the material at certain time t', and is maintained constant in time thereafter. According to this definition, if the specimen is simultaneously subject to drying, temperature changes or other causes of deformation, to measure creep experimentally one must use at least two specimens subject to exactly the same conditions except that one is loaded and the other remains load-free. Creep strains are then equal to the excess strains experienced by the loaded specimen with respect to the unloaded specimen. The dual mechanism of creep is called relaxation, which is the time-dependent reduction of the stress due to a constantly maintained deformational level in time. The resulting strains are partially reversible, which can be measured in a loading/unloading cycle (see figure 3.1b). The proportion of reversible strains depends on many factors, although it is not intended in this study to discuss these issues.

Traditionally, creep has been separated in two superposed strains: a basic creep deformation, which may be defined as the time-dependent deformation under constant load occurring at constant humidity conditions (i.e. the material has a homogeneous distribution of moisture content), and a drying creep strain, defined as the deformation in excess to the basic creep strain observed when the same material is exposed to drying while under load (i.e. there is moisture movement due to lack of thermodynamic equilibrium with the environment). In fact, the water content or internal RH is of paramount importance and plays a paradoxical role in the delayed behavior of concrete and concrete structures (Acker & Ulm, 2001). On one hand, experimental tests performed at hygral equilibrium (i.e. no moisture exchange) show that the lower the evaporable water content within the sample, the lower the observed creep strains (Tamtsia & Beaudoin, 2000; Bazant & Chern, 1985; Wittmann, 1973). On the contrary,

if tests are performed under drying of the specimen, then the higher the moisture difference between the sample and the environment, the higher the observed creep.

The following two definitions used in construction specifications and publications will be used throughout this study:

a) creep coefficient, denoted as $\phi(t, t')$: expresses the delayed deformation with respect to the elastic strain (typical values fall in the range 2.0-6.0, for the maximum attained creep strain);

b) compliance function, denoted as $J(t, t')$: represents the creep strain per unit of imposed stress and is used to compare the delayed strain that takes place in concretes loaded at different stress levels (although the principle of superposition is valid until approximately 30% of the peak load in a compression test); it includes the elastic instantaneous compliance and the creep compliance (also called specific creep);

c) specific creep, denoted as $C(t, t')$: expresses only the delayed strains due to the application of a unit stress (i.e. it excludes the instantaneous elastic strain).

With these definitions, the following relations apply:

$$\phi(t,t') = E(t')J(t,t') - 1 \tag{3.6}$$

$$C(t,t') = \frac{\phi(t,t')}{E(t')} \tag{3.7}$$

$$J(t,t') = \frac{1}{E(t')} + C(t,t') \tag{3.8}$$

in which t' is the age at loading and t is the time at which strains are evaluated. Figure 3.18 shows a schematic representation of various compliance functions for different ages at loading, showing the decrease in time of the instantaneous elastic strain.

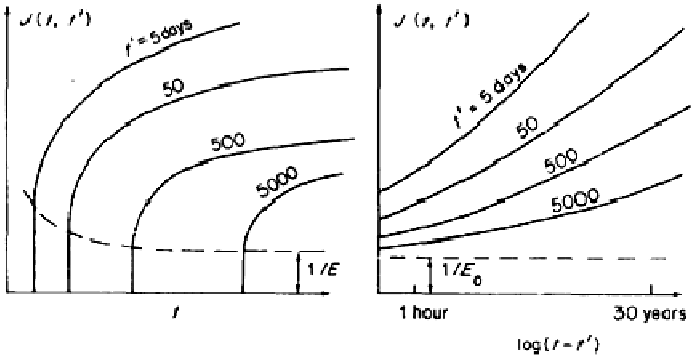

Figure 3.18. Schematic representation of compliance curves for various ages (t') at loading, as a function of time (from Bazant, 1988).

Concrete differentiates from other common materials in civil engineering like steel at elevated temperatures or clay in that creep is approximately linear when subject to a stress level below 30 or 40% of the peak load. In addition, aging effects (i.e. the increase of mechanical properties and evolution of the pore system with time) due to continuous hydration of the cement paste, and a larger relaxation spectrum (hereditary phenomena, with an extended memory) are unique features of cementitious materials.

The origin of these delayed strains in concrete has been the subject of numerous studies, and an appreciable number of different hypotheses have been proposed. Nowadays it is well accepted that the calcium silicate hydrates (CSH in cement

chemistry notation), within the HCP are the main cause behind creep strains (Acker, 2001; Neville, 2002 p. 469; Mehta & Monteiro, 2006). It is also well-known that aggregates, same as in drying shrinkage, reduce and restrain creep deformations (Hua *et al.*, 1997; Neville, 2002). It has been experimentally (by photoelasticity) and numerically determined that during time-dependent deformations there is a redistribution of stress from the HCP to the aggregates (Bolander *et al.*, 2001; López *et al.*, 2001).

3.2.1 Basic creep

As previously outlined, the delayed deformation due to a sustained load in time under equilibrated moisture conditions throughout the material sample is called basic creep and it strongly depends on the moisture content and the drying history (Tamtsia & Beaudoin, 2000), as shown in figures 3.19 and 3.22.

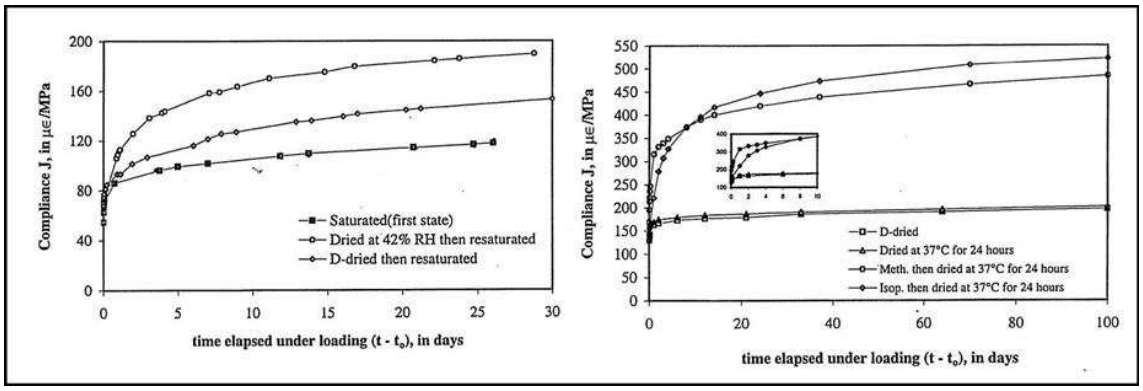

Figure 3.19. Compliance function (microstrain/MPa) of hardened cement paste (w/c=0.5) after (a) resaturation from different drying pre-treatments and (b) after drying pre-treatments without a subsequent resaturation (from Tamtsia & Beaudoin, 2000).

It has been suggested that basic creep shows 2 well-defined stages at the marcoscopical level (Ulm *et al.*, 1999a), given by:

- a *short-term creep kinetics*, acting predominantly during the first days after the application of a load and showing a similar time scale to that of the reversible part of creep strains, suggesting the reversibility of this part of the deformation;
- a *long-term creep kinetics*, characterized by a pronounced aging non-asymptotic period, which seems to depend only on the age of the material and not the age at loading or the loading history.

Figure 3.20 shows these two stages (Ulm *et al.*, 1999a) by plotting the compliance rate as a function of time. Several mechanisms for explaining basic creep of concrete at short or long term have been proposed in the literature. It is not the intention of this work to enter the details of these mechanisms and the avid reader is referred to (Benboudjema, 2002) and (Bazant, 2001). For the case of short term basic creep some of the proposed mechanisms are listed below:

- osmotic pressure effect;
- solidification theory;
- migration of adsorbed water within the capillary porosity.

As for the long term basic creep, the micro-sliding between CSH particles and their own sheets has become a well accepted mechanism (Acker, 2001; Tamtsia & Beaudoin, 2000; Ulm *et al.*, 1999a).

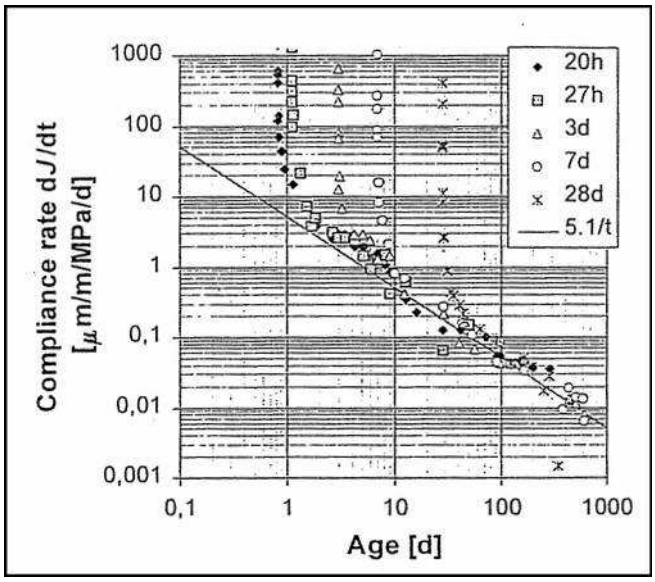

Figure 3.20. Compliance function rate experimentally determined in a conventional concrete of w/c = 0.5 as a function of time (Ulm *et al.*, 1999a).

3.2.2. Drying creep and the Pickett effect

The Pickett effect, named after the first researcher who documented it (Pickett, 1942), is observed when, in addition to a sustained external load, the specimen is subjected to drying. As a result, the total deformation of the sample differs from the sum of the drying shrinkage strains of the load-free sample and the delayed strain due to the application of a sustained load in a non-drying (sealed) specimen (figure 3.21). This means that these two effects cannot be combined by linear superposition. The observed difference between measured strains and strains due to superposed effects is generally non-negligible and it may be interpreted either as a *drying-induced creep* or as a *stress-induced shrinkage*.

Pickett suggested that the excess in the observed deformation is due to a nonlinear relation between stresses and creep strains, which is not theoretically incorrect. However, this simple observation does not allow for a quantification of these extra deformations. Since then, a number of mechanisms to explain the Pickett effect have been proposed in the literature, and some of them have been later discarded due to the disagreement with either theoretical principles or experimental evidence. Among these, the most popular are the seepage theory, the viscous shear theory and the assumption of a micro-sliding between HCP and aggregates. These proposals were not supported by a mathematical model, turning their implementation in numerical models a somewhat arbitrary task. An exception is the assumption of the microcracking effect on the creep strains as the main cause of the excess in total deformation (Wittmann & Roelfstra, 1980). A brief description of each of the proposed mechanisms, as well as the relevant references in the subject can be found elsewhere (Bazant & Chern, 1985; Bazant, 1988; Bazant, 2001; Tamtsia & Beaudoin, 2000). Sixty years after the first publication on this subject, there is still no generally accepted theory, although a lot of progress has been made towards this goal.

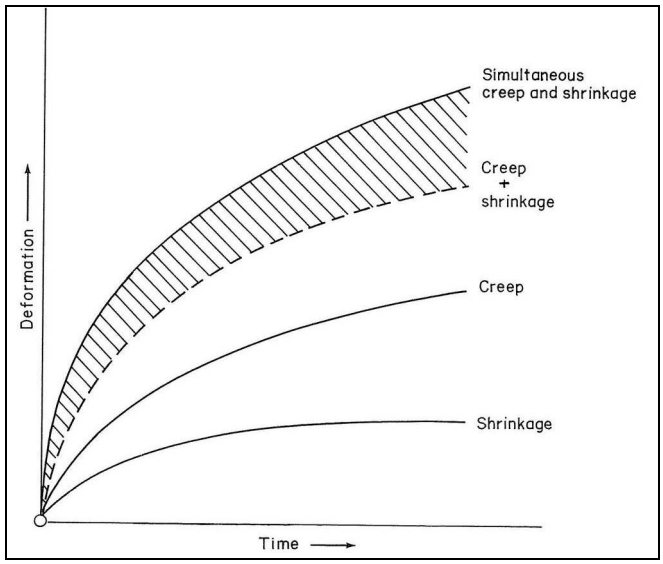

Figure 3.21. Schematic representation of the Pickett effect: drying shrinkage strains, basic creep and the superposition of the two deformations (dashed line), and observable difference (shaded area) between measured strains (from Wittmann, 1982).

The difference between strains measured in experiments and strains resulting from superimposing basic creep and drying shrinkage ones is called drying creep in modern concrete technology and corresponds to the shaded area in figure 3.21. It is known that creep tests are greatly affected by environmental conditions, showing considerable higher strain levels as drying becomes more intense. It is not the ambient humidity *per se* that affects creep, but the intensity of the drying process, driven by the gradient of internal RH (Bazant, 1988). Figure 3.22 shows that this increase can be considerable (Acker & Ulm, 2001).

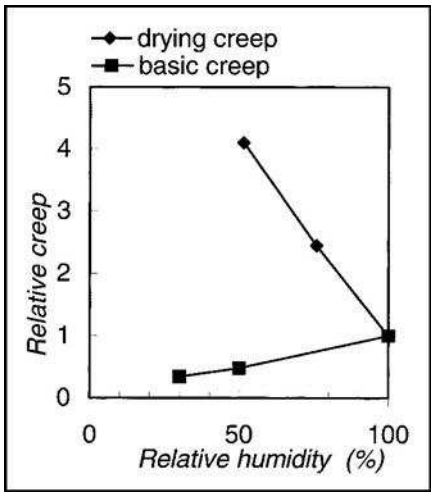

Figure 3.22. Long-term creep for various RH levels (relative to basic creep strains at saturation), showing that low RH values yield lower basic creep deformations but much higher drying creep ones (from Acker & Ulm, 2001).

As stated in previous paragraphs, the mechanisms behind drying creep are still not well understood. However, it is now widely accepted that the total drying creep strain may be subdivided into a structural (or apparent) and an intrinsic part (Bazant & Xi, 1994; Reid, 1993; Benboudjema *et al.*, 2005a). The structural part corresponds to the

drying-induced microcracking (Wittmann, 1982). Accordingly, when a compressive load is acting on the specimen, microcracking will decrease (see e.g. Sicard *et al.*, 1992 and section 3.1.5), thus resulting in an increase of the total strains. On the contrary, when microcracking is not prevented by a compressive load, tensile stresses will develop and form microcracks, thus diminishing these stresses (the material is in a softening regime in the very outer layers). Accordingly, strains will be lower (also the crack opening can be regarded in this case as a tensile strain of the material, while it is under compressive loading). It has been suggested that this effect could explain all of the observed drying creep strains (Wittmann & Roelfstra, 1980). Later studies showed that, although significant, this effect fails to explain a large portion of the total strains (Bazant & Xi, 1994; Thelandersson *et al.*, 1988). In fact, this effect does not explain the experimental observations in very thin specimens (in the order of 1mm), in which RH gradients are minimized (and thus microcracking) and where the Pickett effect is still measured (Day *et al.*, 1984). Another argument against this hypothesis is the fact that drying creep has also been detected in tensile drying creep tests, in which microcracking is not prevented (Kovler, 1999; Kovler, 2001), even though the validity of this last finding is still under discussion (Altoubat & Lang, 2002). Thus, it may be concluded that there must be an intrinsic part of the deformation owing to a material property, yielding a coupling source between drying and creep strains.

Some of the intrinsic mechanisms proposed in past years have been pointed out in previous paragraphs. There have been other proposals exclusively intended to explain drying creep mechanisms. Particularly interesting are the models proposed by:

- Brooks (2001), based on the stress concentration due to the presence of rigid inclusions and macropores;
- Bazant & Chern (1985), who suggested that drying creep can be regarded as stress-induced shrinkage;
- Kovler (2001), who proposed that drying creep is induced by a variation of the curvature radio of the menisci.

The contribution of Bazant and coworkers during the past 30 years has been undoubtedly determining in the modeling of creep and drying shrinkage strains (Bazant & Najjar, 1972; Bazant & Raftshol, 1982; Bazant & Chern, 1985; Bazant, 1988; Bazant & Prasannan, 1989; Carol & Bazant, 1993; Bazant & Xi, 1994; Bazant *et al.*, 1997; Bazant, 2001, among many others). Nowadays, their proposed models, based on the solidification theory for short-term aging (Bazant & Prasannan, 1989) and the microprestress-solidification theory (Bazant *et al.*, 1997), are two of the most cited works in the advance modeling literature, and have been implemented by other researchers (see e.g. Gawin *et al.*, 2007). These theories seem to explain most of the experimental evidence on drying creep. They are based on the assumption that aging acts on the short-term, as a result of the solidification and deposition of stress-free hydration product layers in the pore walls. Long-term creep strains are justified by the theory of relaxation of stresses at the microscopic level (Bazant *et al.*, 1997).

Modeling of drying creep has been finally left out of this thesis, reason by which we will not perform a more exhaustive review on the subject, which can be found elsewhere (Bazant, 1988; Bazant & Chern, 1985; Benboudjema, 2002).

3.3. Code-type formulas for creep and drying shrinkage

In order to predict the experimental results obtained in terms of strains, there are mainly two families of models that should be distinguished. These are 1) true constitutive equations, which describe the behavior of a representative volume element (RVE) of concrete, and 2) models for the approximate overall (mean) behavior of the cross section of a large member (Bazant, 2001). True constitutive equations may be regarded as a description of the deformation which would occur in an infinitesimal element if this element was unrestrained by neighboring elements, and so they must not be confused with the average unit deformation of an unrestrained specimen (Pickett, 1942). The models proposed for the cross-section behavior are inevitably much more complicated in their form, because they must also characterize the solution of the boundary value problem of evolution of humidity distributions, residual stresses and cracking. However, the former models are much more difficult to identify from test data because their fitting to experiments involves an inverse problem. In this section, a summary of the code formulas used in the Spanish code (EHE, 1998) for structural analysis will be presented and constitutive modeling will be reserved for the next section. From a constitutive modeling point of view, code formulas are useful in order to validate constitutive models, when lacking precise experimental data.

The common feature of all code-type formulas is that they try to fit the largest possible amount of experimental data for different concretes with the smallest number of parameters. For the case of drying shrinkage and drying creep, involving a time-dependent diffusion process, an additional parameter regarding the shape and size of the concrete member is included in almost all construction codes. The most relevant construction codes worldwide are the ACI code in theU.S., Canada and Latin America, the Eurocode 2 and CEB-FIP code for Europe, the BPEL 91 from France, the Japanese code and for our study obviously the Spanish code. The input parameters of creep and shrinkage prediction models are generally divided into extrinsic and intrinsic. For all models, the extrinsic ones are the age at the beginning of drying, the environmental RH, the temperature (only in some cases) and the effective thickness of the cross section (usually defined in terms of the volume-to-surface ratio V/S, but also as the ratio between the member's cross-section and its perimeter in contact with the environment). The intrinsic input parameters reflect the composition of concrete and vary from model to model. The most (and sometimes the only) important intrinsic parameter is the standard compression strength at 28 days. Other influencing parameters are the cement content and type, the w/c ratio, the aggregate-cement ratio and other aggregate properties.

3.3.1. Drying shrinkage in the Spanish code (EHE, 1998)

The previous version of the Spanish code (EH-91, 1991) considered drying shrinkage strains in a very simplified manner, ignoring completely any intrinsic property of the concrete material. A newer version has included the compression strength as the only parameter characterizing the material properties (EHE, 1998). Any other intrinsic parameter, like the w/c ratio, will only implicitly be considered through the compression strength. The formulation proposed in this last version is as follows:

$$\varepsilon_{cs}\left(t,t_s\right)=\varepsilon_{cs0}\beta_s\left(t-t_s\right) \tag{3.9}$$

in which t [days] is the time at strain evaluation, t_s [days] is the age at the beginning of drying, ε_{cs0} is the basic shrinkage coefficient and $\beta_s(t-t_s)$ is a coefficient representing the time evolution of shrinkage strains. They can be calculated as

$$\varepsilon_{cs0} = \varepsilon_s \beta_{RH}(RH) \tag{3.10}$$

$$\varepsilon_s = (570 - 5f_{ck}) \cdot 10^{-6}, \text{ with } f_{ck} = \left[N/mm^2 \right] \tag{3.11}$$

$$\beta_{RH}(RH) = -1.55\left(1 - \left(\frac{RH}{100}\right)^3\right) \text{ and } \beta_s(t-t_s) = \left(\frac{t-t_s}{0.035 \cdot e^2 + (t-t_s)}\right)^{0.5} \tag{3.12}$$

$$e = \frac{2A_c}{u} \tag{3.13}$$

In the previous equations, RH is relative humidity (in %), f_{ck} [N/mm^2] is the characteristic compression strength, $\beta_{RH}(RH)$ takes the minimum value of 0.25 for the case of submerged structures, e[mm] is the average thickness (fictitious parameter defining the area exposed to drying), A_c[mm^2] is the area of the cross-section and u[mm] is the perimeter in contact with the environment. It can be noticed that the higher the compression strength of concrete, the lower the shrinkage strains (by its contribution to ε_s), becoming almost negligible for 100MPa compression strength concretes or more.

3.3.2. Creep strains in the Spanish code (EHE, 1998)

Delayed strains due to a stress not exceeding 45% of the compression strength can be calculated with the following code formula, either for the case of basic or drying creep:

$$\varepsilon_{c\sigma}(t,t_0) = \sigma(t_0)\left(\frac{1}{E_{0,t_0}} + \frac{\varphi(t,t_0)}{E_{0,28}}\right) \tag{3.14}$$

in which t [days] is the time at strain evaluation, t_0 [days] is the age at loading, $\sigma(t_0)$ is the applied stress, $E_{0,28}$ is the initial longitudinal modulus of deformation at 28 days (calculated as a function of the average compression strength of the concrete), E_{0,t_0} is the initial longitudinal modulus of deformation at the age of loading and $\varphi(t,t_0)$ is the creep coefficient. In turn, this coefficient can be estimated from the following expression:

$$\varphi(t,t_0) = \varphi_0 \beta_c(t,t_0) \tag{3.15}$$

where φ_0 is the basic creep coefficient given by

$$\varphi_0 = \varphi_{RH}\beta(f_{cm})\beta(t_0) \text{ and } \varphi_{RH} = 1 + \frac{100 - RH}{9.9 \cdot e^{1/3}} \tag{3.16}$$

$$\beta(f_{cm}) = \frac{16.8}{(f_{ck}+8)^{0.5}} \text{ and } \beta(t_0) = \frac{1}{0.1 + t_0^{0.2}} \tag{3.17}$$

and $\beta_c(t,t_0)$ is a function describing the time evolution of creep strains. It is expressed as follows

$$\beta_c(t-t_0)=\left[\frac{(t-t_0)}{\beta_{RH}+(t-t_0)}\right]^{0.3} \quad \text{and} \tag{3.18}$$

$$\beta_{RH}=1.5\cdot e\cdot\left[1+(0.012\cdot RH)^{18}\right]+250\leq 1500 \tag{3.19}$$

It is emphasized that this type of formulation is highly empirical and many extrinsic and intrinsic effects have not been considered. More complete code-type formulas, still of empirical nature but including more intrinsic parameters, can be found elsewhere (Bazant & Baweja, 1995; Gardner & Lockman, 2001; Sakata & Shimomura, 2004).

3.4. Numerical modeling of drying shrinkage in concrete

3.4.1. Different approaches to moisture transfer modeling

Moisture movement and drying of concrete and other porous solids has been studied for a long time (Richards, 1931; Carlson, 1937). When a concrete member is exposed to a lower RH than the internal one, a moisture content gradient is generated near the exposed surface that serves as a driving force for moisture to escape the material, process which is generally known as drying. The drying front thus formed advances towards the interior of the specimen following a diffusion process, which may be expressed by the use of Fick's second law, and can be described in terms of several driving forces used to represent the same phenomenon. Traditionally, the gradients of relative humidity (Bazant & Najjar, 1972; Alvaredo & Wittmann, 1993; Ababneh *et al.*, 2001; Hubert *et al.*, 2003) and evaporable water content (also known as the Richard's equation; see Carlson, 1937; Pihlajavaara & Väisänen, 1965; Granger *et al.*, 1997b; Samson *et al.*, 2005) have been preferred in the literature as driving forces. Moisture is generally present both in its water vapor and liquid phases and it is generally assumed that they coexist in thermodynamic equilibrium at all times for ambient temperatures (Bazant & Najjar, 1972).

More recently, several authors have proposed to analyze drying of porous solids with a multiphase approach, in which the material is considered as a multiphase continuum composed of a solid skeleton and a connected porous space partially saturated by liquid water and an ideal mixture of water vapor and dry air (Bear & Bachmat, 1991; Lewis & Schrefler, 1998; Coussy, 2004; Gawin *et al.*, 2007). In order to obtain such a formulation, the mass balance equations are first derived at the microscopic (pore) level and then upscaled with an average technique. In this way, the equation system is integrated over a representative volume element (RVE), such as the one shown in figure 3.23. A full description of this technique may be found elsewhere (Bear & Bachmat, 1991). The resulting multiphase formulation, i.e. after the averaging procedure, will be presented in the following. Next, it will be shown that by introducing certain assumptions, the simpler formulation in terms of one single driving force (either RH or evaporable water content) can be retrieved. This simplification has already been studied by a number of researchers (Pel, 1995; Mainguy *et al.*, 2001; Witasse, 2000; Meschke & Grasberger, 2003; Samson *et al.*, 2005; de Sa *et al.*, 2008) and the main hypotheses are now well-known. The resulting simplified model, in our case expressing the mass balance in terms of RH, will be adopted throughout this thesis.

It should be noted that the use of a complete multiphase formulation would require the determination of several extra model parameters, some of them of difficult quantification (see e.g. Baroghel-Bouny, 2007). In addition, the uncertainty regarding

pore distribution, connectivity and tortuosity (not to mention the effects of cracking on the transport processes) turns this formulation a more phenomenological than physical representation of the drying process. Nonetheless, its implementation shows some obvious advantages, since it permits to separate the different contributions to the total moisture transport which may be of importance in weakly permeable materials as concrete and under severe conditions (as in the case of fire exposure). A complete analysis of the two formulations as well as a critical assessment has been recently published (Cerný & Rovnaníková, 2002).

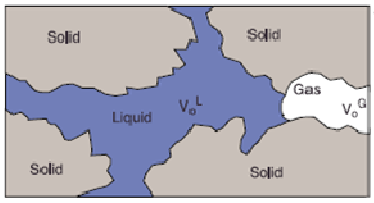

Figure 3.23. Schematic representation of a RVE (representative elementary volume) of hardened cement paste, showing the solid, liquid and gas (dry air + water vapor) phases (after Samson *et al.*, 2005).

As a starting point, the averaged mass balances for liquid water ($_{liq}$), water vapor ($_{vap}$) and dry air ($_{air}$) are first written as

$$\frac{dm_{liq}}{dt} = -div\left(J_{liq}\right) - \dot{m}_{liq\mapsto vap} \tag{3.20}$$

$$\frac{dm_{vap}}{dt} = -div\left(J_{vap}\right) - \dot{m}_{vap\mapsto liq} \tag{3.21}$$

$$\frac{dm_{air}}{dt} = -div\left(J_{air}\right) \tag{3.22}$$

In these expressions, m_i stands for mass content of phase i (per unit volume), t is the time, J_i represents the flux of component i, $\dot{m}_{i\mapsto j}$ accounts for the rate of evaporation/condensation phenomena between liquid water and water vapor (such that $\dot{m}_{liq\mapsto vap} + \dot{m}_{vap\mapsto liq} = 0$). For the following derivation, the hypotheses of incompressible fluid, rigid solid skeleton and negligible effect of gravity are introduced. Assuming that the liquid water flux is driven by a liquid pressure gradient (Darcy's law), and that the gas phase is an ideal mixture driven by a gas pressure gradient (Darcy's law) with diffusion of each component with respect to the other (Fick's law) in an ideal mixture, the fluxes may be written as (Witasse, 2000)

$$J_{liq} = -\frac{\rho_{liq}}{\mu_{liq}} Kk_{rliq}\left(S_{liq}\right) \cdot grad\left(p_{liq}\right) \tag{3.23}$$

$$J_{vap} = -\frac{\rho_{gas}}{\mu_{gas}} Kk_{rgas}\left(S_{liq}\right) \cdot grad\left(p_{gas}\right) - \rho_{gas} D_{vap} \cdot grad\left(\frac{\rho_{vap}}{\rho_{gas}}\right) \tag{3.24}$$

$$J_{air} = -\frac{\rho_{gas}}{\mu_{gas}} Kk_{rgas}\left(S_{liq}\right) \cdot grad\left(p_{gas}\right) - \rho_{gas} D_{air} \cdot grad\left(\frac{\rho_{air}}{\rho_{gas}}\right) \tag{3.25}$$

where ρ_i and μ_i are the mass density and dynamic viscosity for phase i, S_{liq} represents the degree of liquid saturation (1 for fully saturated conditions and 0 for completely dried material), K is the intrinsic permeability of the porous medium (i.e. it does not depend on the fluid traversing it), $k_{ri}(S_{liq})$ is the relative permeability of phase i,

ranging from 0 to 1, which is a function of the degree of saturation, p_{liq} is the liquid pressure and p_{gas} the gas pressure (for an ideal mixture $p_{gas} = p_{vap} + p_{air}$), D_i are the effective diffusion coefficients of component *i* in the mixture (accounting for both tortuosity of the porous system and reduction of the cross section available for diffusion in an empirical way). Note the diffusive terms in the gas mixture, expressed in terms of the mass densities (Witasse, 2000; Samson *et al.*, 2005).

In the following, the capillary pressure is defined by the well-known Kelvin law (describing the thermodynamic equilibrium between the gas and liquid phases), yielding

$$p_c = p_{gas} - p_{liq} = -\rho_{liq} \frac{RT}{M_{wat}} ln(H) \tag{3.26}$$

in which p_c is the capillary pressure, M_{wat} is the water molar mass, T is the temperature (K), R the perfect gas constant and H is the relative humidity, this last variable expressing the ratio between the measured vapor pressure and that at saturation (which depends on the temperature, although in this work we consider isothermal conditions) and is written as

$$H = \frac{p_{vap}}{p_{vap}^{sat}} \tag{3.27}$$

The key assumption for deriving an expression for moisture transfer in terms of a single driving force is that the gas pressure remains constant and equal to the atmospheric pressure, so that $grad(p_g) = 0$ (Pel, 1995; Mainguy, 1999; Mainguy *et al.*, 2001; Witasse, 2000; Samson *et al.*, 2005). The validity of this hypothesis has been discussed in detail elsewhere (Mainguy *et al.*, 2001). It was concluded that in weakly permeable materials as concrete (it is generally valid for more porous materials as soils) this assumption may overestimate the water losses, although it yields a good approximation. With this hypothesis, the dry air conservation equation can be disregarded, as it does not provide any information on the moisture transfer. Moreover, the liquid pressure may be replaced by ($-p_c$), as the gas pressure (assumed to be equal to the atmospheric pressure) can be neglected as opposed to the liquid one. Thus, the flux of liquid water can be rewritten as follows (plugging in eq. 3.26)

$$J_{liq} = +\frac{\rho_{liq}}{\mu_{liq}} Kk_{rliq}(S_{liq}) \cdot grad(p_c) = -\frac{\rho_{liq}^2}{\mu_{liq}} \frac{Kk_{rliq}(S_{liq})}{M_{wat} H} \cdot grad(H) \tag{3.28}$$

The degree of saturation (S_l) may be expressed, for convenience, as a function of RH (H) through the desorption isotherms (or water retention curves, as shown in section 3.1.3). In this way, the relative permeability can be written as $k_{rl} = k_{rl}(H)$.

The equation of state of perfect gases and Dalton's law are assumed for the dry air, water vapor and their mixture, yielding

$$\rho_{gas} = \rho_{vap} + \rho_{air} \text{ and } p_i = -\frac{RT}{M_i} \rho_i \text{ for } i = air, vap, gas \tag{3.29}$$

Thus, ρ_{gas} may be written as

$$\rho_{gas} = \frac{\left(M_{air}\, p_{air} + M_{wat}\, p_{vap}\right)}{RT} = \frac{\left[M_{air}\, p_{gas} + \left(M_{wat} - M_{air}\right) p_{vap}\right]}{RT} \tag{3.30}$$

Plugging in the expressions for ρ_{gas} and p_{vap} in eq. 3.24, the vapor flux is rewritten as

$$J_{vap} = -\rho_{gas} D \cdot grad\left(\frac{\rho_{vap}}{\rho_{gas}}\right) = -\rho_{gas} D \cdot grad\left[\frac{M_{wat}\, p_{vap}}{M_{air}\, p_{gas} + \left(M_{wat} - M_{air}\right) p_{vap}}\right] \tag{3.31}$$

After some straightforward derivation, equation 3.31 is expressed as

$$J_{vap} = -\frac{\rho_{gas} D M_{wat} M_{air}\, p_{gas}}{\left[M_{air}\, p_{gas} + \left(M_{wat} - M_{air}\right) p_{vap}\right]^2} \cdot grad\left(p_{vap}\right) \tag{3.32}$$

Plugging in equation 3.30 and considering that $p_{vap}^{sat} H = p_{vap}$ (from eq. 3.27)

$$J_{vap} = -\frac{D M_{wat} M_{air}\, p_{gas}\, p_{vap}^{sat}}{RT\left(M_{air}\, p_{gas} + \left(M_{wat} - M_{air}\right) p_{vap}^{sat} H\right)} \cdot grad\left(H\right) \tag{3.33}$$

The total moisture transport may be calculated by adding up the liquid and the water vapor fluxes given in eqs. 3.28 and 3.33, yielding (for $p_{gas} = p_{atm}$)

$$J_{total} = -\left[\frac{D M_{wat} M_{air}\, p_{atm}\, p_{vap}^{sat}}{RT\left(M_{air}\, p_{atm} + \left(M_{wat} - M_{air}\right) p_{vap}^{sat} H\right)} + \frac{\rho_{liq}^2}{\mu_{liq}} \frac{Kk_{rliq}\left(H\right)}{M_{wat} H}\right] \cdot grad\left(H\right) \tag{3.34}$$

The term in brackets in eq. 3.34 may be recognized as the nonlinear effective diffusion coefficient $D_{eff}(H)$, which depends on the porous medium characteristics through K and D, as well as on the RH (H) itself. Moreover, since the driving force in this formulation is the gradient of RH, it is convenient to express the variation of moisture content in terms of this variable, in order to obtain the mass balance as a function of only the RH Adding up the mass balances for liquid water ($_{liq}$) and water vapor ($_{vap}$) yields

$$\frac{d\left(m_{liq} + m_{vap}\right)}{dt} = \frac{dw}{dt} = \frac{dw}{dH} \cdot \frac{dH}{dt} = -div\left(J_{total}\right) \tag{3.35}$$

in which w represents the total moisture content. Note that the rates of evaporation and condensation cancel each other. The derivative of the moisture content with respect to H can be calculated as the slope of the desorption isotherm and is often referred to as the moisture capacity matrix and denoted as $C(H)$ (Xi *et al.*, 1994b). Finally, the transport of moisture through the porous concrete material is expressed, in its simplified form, as

$$C\left(H\right) \cdot \frac{dH}{dt} = -div\left(D_{eff}\left(H\right) grad\left(H\right)\right) \tag{3.36}$$

There is still another hypothesis usually introduced in this type of models. Namely, the moisture capacity is assumed constant within the range 50-100% RH, arguing that the slope of the desorption isotherm in this part of the curve is approximately constant. In this case, eq. 3.36 may be finally written as

$$\frac{dH}{dt} = -div\left(\tilde{D}_{eff}\left(H\right) grad\left(H\right)\right) \tag{3.37}$$

in which $\tilde{D}_{eff}$ gathers the diffusion coefficient and the moisture capacity matrices.

The most salient feature of equation 3.37 consists of the strong dependence of the diffusion coefficient on the RH (Bazant & Najjar, 1972), which was already suggested in the 1930's by Carlson (1937). As shown in the previous derivation of equation 3.37, the nonlinear effective diffusion coefficient gathers different transport phenomena, allowing us to express the drying process as a function of a single driving force. As a consequence, theoretical or analytical evaluation of this coefficient has not been pursued in the literature. Instead, different nonlinear expressions have been proposed to relate diffusivity with RH (or, alternatively, moisture content or degree of saturation) in order to fit experimental data, although they all show similar trends (see e.g. Roncero, 1999 for a review of some proposals). In this work the expression proposed by Roncero (1999) has been preferred, as will be shown in Chapter 4. We emphasize that all of these expressions are of empirical nature and give an *effective* diffusion coefficient, since the overall moisture movement is composed of different mechanisms of difficult quantification. A complete review on this subject has been presented elsewhere (Xi *et al.*, 1994a,b).

As stated above, other authors have proposed to analyze the drying process in terms of the evaporable water content as the only driving force (Pihlajavaara & Väisänen, 1965; Granger *et al.*, 1997b; Thelandersson, 1988; Torrenti *et al.*, 1999; Benboudjema *et al.*, 2005a; Samson *et al.*, 2005). According to Bazant & Najjar (1972), the use of RH as the state variable yields certain advantages:
- in moderate to high w/c ratios (i.e. excluding the case of high performance concrete), the decrease in internal RH due to self-desiccation is negligible (a few percents at the most), which is not the case for the non-evaporable water content (unless the hydration period is completed);
- initial and boundary conditions are expressed more naturally in terms of RH (see Granger *et al.*, 1997b and the following paragraphs);
- when generalizing the formulation to a non-isothermal analysis, the RH may still be used as a driving force for moisture transport, whereas the water content has some deficiencies (Xi *et al.*, 1994a).

On the other hand, the following justifications are often stated by those considering the water content (Granger *et al*., 1997):
- moisture content (quantified by the moisture loss) is easier to measure experimentally than RH; however, the measured quantity is the overall moisture loss, which does not give any information on the local moisture conditions;
- the shrinkage coefficient (see next subsection) may be easily identified from the linear portion of the shrinkage vs. overall weight loss curve;
- for low quality concretes of high w/c ratios (higher than roughly 0.6) the slope of the desorption isotherm curve is too steep near water saturation, yielding the use of water content a more convenient choice in these exceptional cases.

It should be emphasized that both formulations yield good results and the main differences are more of practical importance than theoretical nature. In fact, both formulations make use at some point in the analysis of the well-known desorption isotherms (see section 3.1.3) to relate the RH with the moisture content (i.e. the state variables in these two approaches). In this thesis the expression proposed by Kristina Norling has been adopted (Norling, 1994; Norling, 1997). It considers the degree of hydration, the w/c ratio and the cement content as input material variables for this relation (see Chapter 4).

3.4.2. Boundary conditions

To complete the formulation, the boundary conditions should be specified. For the case of RH as the driving force, the different possibilities are to fix the value of the variable on a exposed surface (Dirichlet type boundary condition, representing perfect moisture transfer, eq. 3.38), to impose the flux normal to a surface (Neumann boundary conditions, mostly used for this application to represent a sealed surface with zero normal flux, eq. 3.39), and to impose a convective boundary condition (also called Robin condition), to account for an imperfect transfer of moisture between the environment and the concrete surface (see eq. 3.40).

$$H = H_{env}(T,t) \tag{3.38}$$

$$\frac{\partial H}{\partial n} = f(T,t) \tag{3.39}$$

$$grad(H) = \beta(H - H_{env}) \tag{3.40}$$

In the previous equations, T is the temperature, t is the time, H_{env} the environmental RH, n the normal vector to a given surface and β the surface emissivity (note that as $\beta \to 0$, $H \to H_{env}$, recovering the Dirichlet boundary condition). The surface emissivity depends on air velocity, porosity, surface roughness, etc., and it should be determined in experiments (Pel, 1995; Torrenti *et al.*, 1999). On the contrary, this coefficient seems to be independent of the value of environmental RH (Ayano & Wittmann, 2002). In any case, the influence of this parameter is rather subtle (see for instance van Zijl, 1999) and it is also usual practice to consider the perfect moisture transfer condition, as in eq. 3.38 (see e.g. Bazant & Raftshol, 1982; Bazant, 1988, Chapter 2). From a numerical point of view, the use of a finite value for the surface emissivity (a typical value of 5mm/day is usually adopted, see Witasse, 2000) has some advantages, as it reduces the sharp humidity gradient at the beginning of drying, thus obtaining a faster convergence and a considerable reduction of oscillations in the solution (van Zijl, 1999).

3.4.3. Modeling shrinkage strains

One of the main issues for which there are still certain uncertainties, despite a lot of effort dedicated to its determination, is the modeling of shrinkage strains in a hygro-mechanical analysis. The problem has been to establish a relation, at a local level (i.e. at the material level), between the moisture loss or change in RH and the resulting volumetric shrinkage strains (see e.g. figure 3.4). This is mainly due to the fact that experimental measurements of shrinkage strains are affected by different kind of restrictions of the samples used in most cases, which cause an alteration of the strain field due to skin microcracking of the sample (see section 3.1.5). Our inability to measure a totally unrestrained shrinkage strain prevents us from extrapolating the material (local) behavior to the structural (overall) one. Nonetheless, it has been generally accepted that the best way to minimize this restrictions is to use very thin (in the order of 1mm or less) HCP specimens (Hwang & Young, 1984). The reason to employ thin samples is to reach hygral equilibrium in a reduced time, so as to reduce shrinkage-induced stresses. A theoretical study by Bazant & Raftshol (1982) let them conclude that microcracking occurs even in the case of very thin samples, which was later confirmed experimentally (Hwang & Young, 1984). Recently, interesting experimental results have been presented that clearly show the effect of restrictions on

the shrinkage strains (Ayano & Wittmann, 2002). They performed drying shrinkage tests (45% RH) in prismatic concrete specimens of $100x150x33mm^3$ (16mm max. aggregate size) of two types: some of them were sliced in 3mm thick slices and dried together as a block (in the spirit of figure 3.11b), so as to minimize restrictions in each layer (see figure 3.24b), and the other ones were kept as solid specimens (i.e. without slicing). In this way, the shrinkage strain profiles they obtained in the first case were closer in shape to the measured RH profiles than in the case of solid specimens, due to a high reduction of the restriction, as shown in figure 3.24a. As a result, a power law was proposed for the dependence of the shrinkage coefficient on the RH, which should be fitted experimentally for each case.

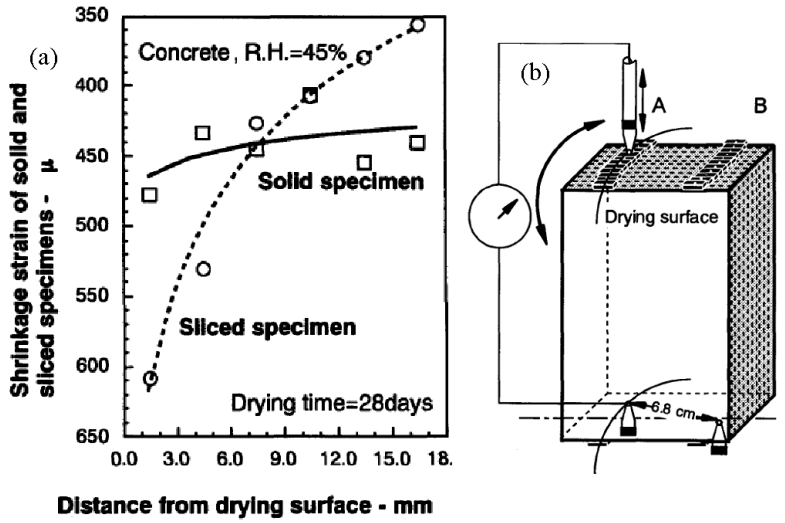

Figure 3.24. (a) Shrinkage strains as a function of the distance from the drying surface for prismatic solid concrete specimens of $100x150x33mm^3$ and sliced (otherwise the same) specimens allowing for approximately unrestrained shrinkage of each slice of 3mm thick; (b) schematic representation of the sliced samples (adapted from Ayano & Wittmann, 2002).

Of course, as a first approximation a linear relationship between strains and weight losses (or in some cases RH) could be adopted (Alvaredo & Wittmann, 1992; Benboudjema *et al.*, 2005a; López *et al.*, 2005b). The constant shrinkage coefficient in this case could be determined as the slope of the linear part of the longitudinal strain vs. weight loss curve, easily measured in a drying shrinkage test (see e.g. Granger *et al.*, 1997b). Several authors suggest that the best way available today for obtaining the shrinkage coefficient is by inverse analysis in a numerical simulation of drying shrinkage tests (see for instance Bazant & Xi, 1994). In this context, it has been proposed to relate this coefficient to RH in a nonlinear way (Alvaredo, 1995; van Zijl, 1999), to weight losses (Martinola *et al.*, 2001) and to the age of the material (Bazant & Xi, 1994). In this thesis, a constant value of the shrinkage coefficient has been adopted for most of the calculations, with a value of $0.01cm^3/gr$ in agreement with data found in the literature (Torrenti & Sa, 2000; Benboudjema *et al.*, 2005b). However, it will be shown in the next chapter that a nonlinear relationship may be more realistic when fitting experimental data, as determined by inverse analysis.

Finally, some authors have preferred to study drying shrinkage within the framework of the well-established theory of poroelasticity (Coussy, 2004). In this case, shrinkage is imposed as a pore pressure of the liquid water and moist air compressing the solid and

thus causing shrinkage. The equivalent of the shrinkage coefficient in this formulation is the Biot coefficient that takes into account the ratio of bulk moduli for solid phase and the skeleton (Gawin *et al.*, 2007). A detailed description of this formulation in the context of concrete mechanics is out of the scope of this thesis and may be found elsewhere (Coussy *et al.*, 1998; Coussy, 2004; Mainguy *et al.*, 2001). Using poroelasticity theory, a nonlinear relation between shrinkage strains and RH has been derived (Baroghel-Bouny *et al.*, 1999). Other proposals include the modeling of shrinkage through capillary pressure (Yuan & Wan, 2002), or capillary pressure and disjoining pressure (Han & Lytton, 1995).

3.4.4. Modeling moisture movement through open cracks

Flow through discontinuities has been the subject of numerous studies over the last 40 years, the main field of application being the assessment of permeability of fractured rock masses (Berkowitz, 2002; Segura, 2007). The need for determining the influence of cracks on the transport processes is also present in concrete mechanics, and a lot of experimental work has been devoted to determine the permeability and/or diffusivity of the cracked material, as shown in previous sections. From a modeling point of view, there have been traditionally three numerical approaches to study flow through porous media with discontinuities. Those are the equivalent continuum approach, the double continuum approach and the discrete approach. A review of the different type of approaches, mostly used in fractured geological media, can be found elsewhere (Roels *et al.*, 2003; Segura, 2007). In short, the equivalent continuum medium may be used when the domain of interest is large enough as compared to the spacing between fractures and small enough as compared to the scale of the problem. It replaces the discontinuous domain by a continuum that averages the overall properties. Double-continuum models make a distinction between the flow through the continuous matrix and through the discontinuities, characterized by their own hydraulic properties, by overlapping two continuous mediums (each one representing the uncracked material and the discontinuities). Finally, the discrete crack approach considers explicitly each discontinuity present in the fractured media. The model used in this thesis falls in this last category.

In this section a brief discussion of the most relevant model procedures within the framework of concrete durability assessment will be addressed, and an additional group of numerical approaches in the above mentioned classification will be presented, originated perhaps as a consequence of the strong influence that fracture and damage mechanics have had on the coupled hygro-mechanical analysis of cracked concrete. Contrary to the field of fractured geological media, in which the mechanical aspect has often not been given a lot of attention, within the concrete mechanics community the models initially proposed to analyze the pure mechanical behavior have had to be adapted for the case of hygro-mechanical coupling. With this in mind, a straightforward distinction between explicit (either numerical or theoretical) models, taking into account fractures in an explicit way and damage or smeared-crack models (considering the presence of cracks in an implicit or diffuse way) is suggested for differentiating several approaches found in the literature. This is obviously in concordance with the crack representation classification proposed in Chapter 2, namely the discrete crack and the smeared crack approaches.

3.4.4.1. Explicit models

Traditionally, in order to explicitly quantify the conductivity or diffusivity along a single crack, the cubic law (also known as Poiseuille law) has been used (Snow, 1965).

It expresses the relation between the diffusion or conductivity coefficient within a crack and the third power of the crack width (Bazant & Raftshol, 1982; Meschke & Grasberger, 2003; Segura & Carol, 2004; Segura, 2007). It has been obtained by considering an idealized laminar flux between two parallel smooth plates. The physical crack width may be replaced by an equivalent hydraulic crack width, representing the aperture of a parallel plate fracture that has the same conductivity as the actual crack. Many authors agree that the cubic law is nowadays the best modeling tool available for studying flux through discontinuities, even though its applicability to very rough surfaces and non-saturated states is still open to debate (Berkowitz, 2002; Segura, 2007). In fact, it has been argued that for very small crack openings the validity of the cubic law is rather questionable when compared to experimental data (Sisavath *et al.*, 2003; Segura, 2007). It has been observed that in this case the conductivity of liquid flow decreases more rapidly that the cube of the aperture. Recently, some modifications to the classical cubic law have been proposed in order to extend its applicability, although the implementation is of a considerable complexity (Sisavath *et al.*, 2003). Cracks were idealized as two sinusoidal surfaces with varying mean aperture, amplitude and wavelength. It is argued that a more rigorous representation of flow through a crack should consider crack roughness and variations in aperture whenever roughness is of the same order of magnitude as the mean aperture. The model proposed in that work, however, cannot capture the flow through very narrow cracks (for a few tens of microns). A complete review of the validity of the cubic law for liquid flow due to a pressure head, lying mostly in the field of rock mechanics, and a discussion of its main features are out of the scope of this thesis and can be found elsewhere (Segura, 2007). Hereafter we focus our attention on some efforts made in the field of concrete mechanics in order to quantify and determine the importance of moisture escape through microcracks.

One of the first studies in this field was presented by Bazant and coworkers. They proposed a simplified upper bound theoretical model, based on the cubic law and the crack system of figure 3.17b, for estimating the influence of cracks on the drying process in terms of water vapor and determined an increase in the effective diffusivity of the medium of several orders of magnitude for cracks openings of 300 microns and 30cm spacing (Bazant & Raftshol, 1982). However, drying shrinkage-induced cracks of 10 microns were determined to only double the diffusion coefficient. They also derived an expression showing the dependency of the diffusivity on the square of the crack penetration, concluding that the effect of cracks must be negligible at the beginning of drying. This study was based on rather crude approximations of the different parameters involved, reason by which it should only be considered to indicate a trend line of the real behavior.

Another theoretical analysis of diffusion through cracks was performed in (Gérard & Marchand, 2000). In this case an expression for the diffusivity along the crack was not provided and only a sensitivity analysis of the different relationships established therein was carried out. They considered two simplified cases of traversing cracks in one and two perpendicular directions (see figure 3.25a,b), the results obtained thus being only rough estimates of the upper bounds of the studied effect. The increase in the apparent diffusivity of the cracked material was significant and depending on the crack spacing and the ratio between diffusivity through the crack (taken to be equal to the diffusion coefficient of an ion in free solution) and that of the uncracked material (figure 3.25c). One interesting conclusion of this work is that cracking is relatively more important for

dense materials (having a low porosity), which is a common feature of fractured rock masses (permeability in these cases is entirely driven by flow through the crack system).

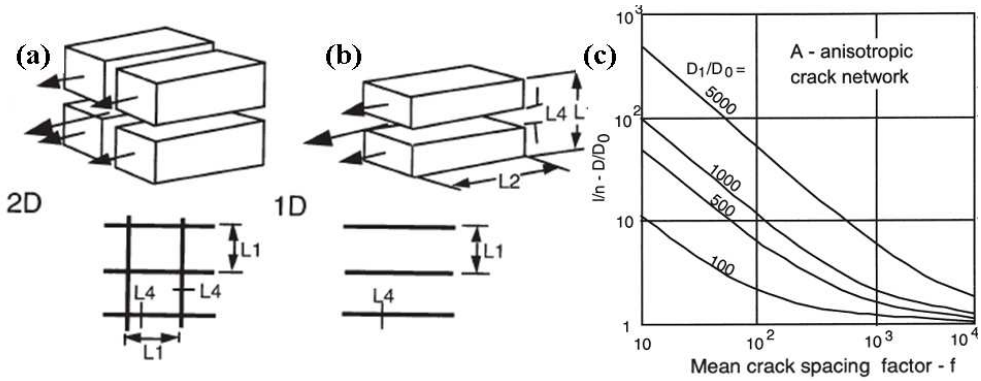

Figure 3.25. Theoretical analysis by Gérard & Marchand (2000): schematic representations of the two crack patterns considered in their study: (a) isotropic 2D cracking and (b) anisotropic 1D cracking; (c) variation of the diffusivity of the cracked material as a function of the ratio between diffusion through the crack and uncracked material (D_1/D_0) and the ratio L_1/L_4=f (adapted from Gérard & Marchand, 2000).

More recently, a theoretical analysis of the coupled diffusion-dissolution phenomenon (with small or no convective flux) in reactive porous media, such as concrete or cement paste subjected to leaching (dissolution of portlandite), was presented, in which the effect of a single narrow crack (with a high length to width ratio) on the process rate is studied with dimensional analysis (Mainguy & Ulm, 2001). They concluded that for small crack openings the process slows down in time, as the diffusion in the crack is not sufficiently intense to evacuate the increase in solute that arrives through the fracture walls, leading to a 'diffusive solute congestion' in small fractures. These findings suggest that the presence of microcracks will not significantly accelerate the overall dissolution (or precipitation) or penetration kinetics of aggressive agents in porous materials.

Carmeliet and coworkers studied moisture uptake in fracture porous media with a combination (coupling) of a 1D discrete model for liquid flow in a fracture (*via* the moving front technique and assuming the cubic law) with a FEM that solves the unsaturated liquid flow in the porous matrix (Roels *et al.*, 2003; Moonen *et al.*, 2006). Although this seems an interesting approach, the determination of the total flow requires the coupled solution of two different techniques (FEM and moving front technique). Its applicability in cases of crack propagation with *a priori* unknown paths is not straightforward (and this type of analysis has not been attempted), and the analysis of moisture diffusion has not been discussed by the authors.

3.4.4.2. Damage and smeared-crack models

There is a second approach when considering microcracking effects on the drying process. Namely, a few authors have preferred to tackle this problem within the framework of the well-known continuum damage theory. In this type of models, microcracks are only implicitly defined in a continuum approximation. Quantifying the effect of microcracks in this case is not an easy task, due to the difficulty in identifying the crack apertures (Dufour *et al.*, 2007). One possibility is to introduce a single damage variable of empirical nature for this purpose (Ababneh *et al.*, 2001), and assuming that drying-induced microcracking is isotropic. Coupling is considered by multiplying the

effective diffusivity of the medium by a factor $(1\text{-}d)^{-1}$, where d is the mechanical damage variable. The assumption of considering a unique damage variable affecting in the same way the mechanical stiffness and the moisture diffusivity seems a rather crude hypothesis. Additionally, the effect of the differential shrinkage between aggregate and cement paste may alter the moisture capacity (derivative of the desorption isotherm) of concrete and thus introduce a second source of coupling, which has been studied by using non-equilibrium thermodynamics and the minimum potential energy principle (Ababneh *et al.*, 2001). Another method to incorporate the effect of damage on the diffusivity is to use the concept of composite damage mechanics (Xi & Nakhi, 2005; Suwito *et al.*, 2006), in which the damaged and the sound fractions of the material are considered as different phases. The main difference with the previous approach is that the damaged fraction is not considered as a void but as a damaged material with increased diffusivity. Results obtained with these models (Suwito *et al.*, 2006) show a small but appreciable influence of the damage due to drying shrinkage on the drying process (i.e. the coupling effect). These models can be regarded as included in the equivalent continuum type, in which the fractured material is interpreted as an equivalent continuous medium.

Within the framework of hygro-mechanical analysis of concrete and a smeared crack approach (see Chapter 2) for representing a fracture, Meschke and Grasberger (2003) recently proposed an alternative way of analyzing flow through a crack based on the analogy between the smeared crack concept and the distribution of the moisture flow along a single crack within the cracked element. In this way they proposed an additive decomposition of the (anisotropic) permeability tensor into two portions considering flow through the porous sound material and through the crack, in this last case *via* the cubic law. The main difficulty of using such an approach is the determination of the crack width (in their work they make use of the hydraulic width concept) in the context of smeared deformations. To accomplish this task they ingeniously established an analogy between the crack in a continuous medium and a uniaxially stretched bar containing a fracture. The crack width is obtained as the difference between the total elongation of the bar and the change of length of the intact unloading parts of the bar. As a result, a relation between the crack aperture and the damage state of the element (given by an internal variable for tensile damage) can be retrieved. Crack width of the order of several tens of mm have been obtained in a durability analyses of a tunnel shell subjected to thermal and hygral gradients cycles (Grasberger & Meschke, 2004). Unfortunately, its application to diffusivity (not permeability) through narrow cracks has not been attempted. Moreover, the crack widths obtained in this way may not be very realistic, due to the simplifying assumptions made to derive this formulation.

More recently, a similar approach, although more sophisticated, for the analysis of permeability of cracked concrete within the framework of damage mechanics has been proposed (Chatzigeorgiou *et al.*, 2005; Choinska *et al.*, 2007; Dufour *et al.*, 2007). Crack opening is also related to the internal damage variable. They proposed to divide the relation between permeability and damage in regions of different behavior, arguing that this relation may be fitted with a phenomenological exponential law in the range of diffuse microcracking. When strain localization takes place in a narrow band (macrocracking), they assumed that the cubic law should be used instead, with a soft transition between these two modes. However, as stated in their paper, the hypotheses on which computation of the crack opening is founded are disputable. Indeed, a reliable way to extract a crack opening from a damage model is missing and is still not usual practice, although the advances cited in this section are promising.

These models do not fit in any of the commonly proposed categories mentioned in previous paragraphs for representing flow through discontinuities. This is due to the fact that their derivation obeys the need of extending the applicability of existent mechanical models to analyze flow through fractured porous media. It is suggested here that they could represent a fourth category in the previous classification.

3.5. Numerical modeling of creep in concrete

3.5.1. Constitutive modeling of basic creep

In the case of basic creep modeling of concrete it is generally accepted to assume a linear relation between stress and strain, provided that stresses are not larger than 30 to 50% of the compression strength, approximately. This relation may be written as follows

$$\varepsilon_i(t) = \sigma_i \cdot B \cdot J(t,t') + \varepsilon_i^0(t) \tag{3.41}$$

in which $J(t,t')$ is the compliance function (as defined in section 3.2), *t'* is the age at loading, *t* is the time at which strains are evaluated, $\varepsilon^0(t)$ represents the stress-independent strains (e.g. drying shrinkage and thermal strains), with only volumetric components and *B* is a matrix containing the Poisson effect, introduced to generalize the formulation to the 2D or 3D case (assuming isotropic behavior) and expressed by

$$B = \begin{bmatrix} 1 & -\nu & -\nu & 0 & 0 & 0 \\ -\nu & 1 & -\nu & 0 & 0 & 0 \\ -\nu & -\nu & 1 & 0 & 0 & 0 \\ 0 & 0 & 0 & 1+\nu & 0 & 0 \\ 0 & 0 & 0 & 0 & 1+\nu & 0 \\ 0 & 0 & 0 & 0 & 0 & 1+\nu \end{bmatrix} \tag{3.42}$$

Assuming the Boltzmann superposition principle as valid, which is usual practice for low stress levels and implies a linear elastic constitutive relation, the previous equation may be generalized to

$$\varepsilon_i(t) = \int B \cdot J(t,t') \cdot \mathrm{d}\sigma_i(t') + \varepsilon_i^0(t) \tag{3.43}$$

which can be implemented for an aging viscoelastic material. Analogously, the *relaxation function* can be expressed as:

$$\sigma_i(t) = \int B^{-1} \cdot R(t,t') \cdot \left[\mathrm{d}\varepsilon_i(t') - \mathrm{d}\varepsilon^0(t) \right] \tag{3.44}$$

In the previous equation *R(t,t')* is the relaxation function (decrease of stresses due to a constant unitary strain) and $d\varepsilon^0$ has been subtracted since by definition it does not induce any stress. A typical schematic representation of this function for various ages at strain imposition can be seen in figure 3.26.

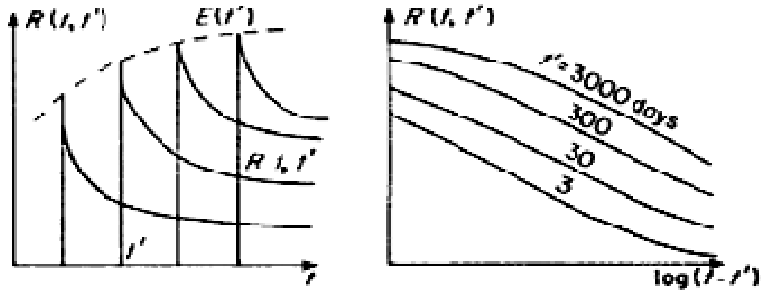

Figure 3.26. Schematic representations of the relaxation function for various ages (t') at strain imposition, as a function of time (from Bazant, 1988).

In the case of basic creep it may be assumed that the Poisson coefficient (ν) remains constant, which in fact has been considered in this thesis (Bazant, 1988). However, for drying creep this hypothesis may not be valid and a more rigorous evaluation in terms of RH should be performed (Benboudjema, 2002).

The previous equations (eqs. 3.43 and 3.44) are in their integral form. From a computational viewpoint this fact requires the expensive storage of the entire stress history in order to numerically evaluate these integrals. An attractive alternative, much more efficient, is to approximate the integral-type expressions with rate-type relations between stresses and strains. These last are based on Kelvin or Maxwell chains with an arrangement of springs and dashpot units used to model aging viscoelasticity. The advantage is that the loading history is expressed in this case by the current values of a predetermined number of internal variables (Carol & Bazant, 1993). To this end, the relaxation function (or its dual compliance function) is replaced by a series of exponential real functions or Dirichlet series (also referred to as Prony series), which take the following form:

$$R(t,t') = \sum_{\mu=1}^{N} E_\mu(t') \cdot e^{\left(y_\mu(t') - y_\mu(t)\right)} \tag{3.45}$$

where $E_\mu(t')$ is now a function of only one variable, $y_\mu(t) = (t/\tau_\mu)^q$, with $0 < q \leq 1$ and τ_μ is the so-called relaxation time. In the case of an aging material, as concrete, the use of the relaxation function is more convenient in order to convert the integral formulation into a differential-type relation, since the transformation of the compliance function yields a second order differential equation, while with the former a first order differential equation is obtained (Bazant, 1988). In addition, it can be shown that the Maxwell chain model comes out naturally from the formulation in terms of the relaxation function (see e.g. Ozbolt & Reinhardt, 2001).

A more physical approach to describe the aging effect of concrete has been proposed by Bazant and coworkers (Bazant & Prasannan, 1989; Bazant *et al.*, 1997). They suggested that the increase of the strength in time is not just a function of the age of the material *per se* but that it depends on two factors (see also Ulm *et al.*, 1999a). On one hand the gradual deposition of new CSH layers as hydration products provoke part of the effect, although this process cannot explain by itself all the aging effect. Thus, as a second factor with a different time scale, they introduced the concept of micro-prestress solidification theory (Bazant *et al.*, 1997), based on the assumption of a relaxation of preexistent stresses at the microscopic level, transverse to the slip plane of CSH sheets, yielding a purely mechanical effect and acting in the long term. Although this model is one of the most advanced proposals for studying basic and drying creep, it does not

consider the role that RH plays in the basic creep strains, as discussed in section 3.2.1 (Bazant & Chern, 1985; Acker & Ulm, 2001).

This last experimental evidence has been considered in a recent model proposed for the modeling of basic and drying creep of concrete (Benboudjema, 2002; Benboudjema *et al.*, 2005b), which exploits some observations done by others on wood materials (said to behave in a similar way regarding creep strains). In this model, the effect of humidity on basic creep is simply added by multiplying the creep function by the local RH value. It should be noticed that a humidity dependent viscosity entering the Maxwell chain for equilibrated RH conditions has also been proposed elsewhere (Bazant & Chern, 1985).

In this thesis, a Maxwell chain model has been adopted for which the chain parameters have been adjusted in order to fit the compliance function for concrete given in the Spanish code (EH-91, 1991, EHE, 1998). Only the case of basic creep under saturated conditions is considered in this thesis. No coupling with RH conditions is introduced in this first attempt.

3.5.2. Some final remarks on modeling drying creep

In section 3.2.3 it has been shown that drying creep strains are the result of two contributions: a structural or apparent part, which is due to microcracking occurring at low RH, and an intrinsic part of the deformation, which is due to internal physico-chemical mechanisms taking place due to the drying process. At present, and although a lot of progress has been made in recent years, there is no general consensus on the exact origin of these strains (Ulm *et al.*, 1999a; Acker, 2001). From a modeling point of view, it has been proposed to consider the intrinsic part of drying creep as a stress-induced shrinkage (Gamble & Parrot, 1978; Sicard *et al.*, 1996; Bazant & Chern, 1985; Bazant & Xi, 1994). Drying creep strains are thus expressed as

$$\varepsilon^{dc}(t) = \mu_{fd} \cdot \varepsilon^{sh} \cdot \sigma \tag{3.46}$$

where ε^{dc} is the drying creep strain, μ_{fd} is a constant material parameter and ε^{sh} is the humidity dependent drying shrinkage deformation. A physical argument supporting this dependency was proposed by assuming that the viscosity of the material depends on RH (Bazant & Chern, 1985; Bazant & Xi, 1994), yielding

$$\frac{1}{\tilde{\eta}} = \frac{1}{\eta} - \alpha_{sh} dH \tag{3.47}$$

in which $\tilde{\eta}$ is the moisture dependent viscosity entering the rheological model (a Kelvin chain model in their proposal), η is a constant viscosity independent of RH, α_{sh} is the drying shrinkage coefficient and dH represents the RH change. Note that viscosity multiplies the stress tensor in the constitutive equation, thus yielding a term similar to equation 3.48. Another theory was proposed later, called the *micro-prestress solidification theory* (Bazant *et al.*, 1997). The idea is that a relaxation of these micro-prestresses, acting in the zones of hindered adsorption of water, causes drying creep stresses. A complete review of drying creep models was recently published elsewhere (Benboudjema, 2002) and will not be attempted in this review.